



CERN-EP-2022-065
24 March 2022

Measurement of beauty-strange meson production in Pb–Pb collisions at $\sqrt{s_{NN}} = 5.02$ TeV via non-prompt D_s^+ mesons

ALICE Collaboration*

Abstract

The production yields of non-prompt D_s^+ mesons, namely D_s^+ mesons from beauty-hadron decays, were measured for the first time as a function of the transverse momentum (p_T) at midrapidity ($|y| < 0.5$) in central and semi-central Pb–Pb collisions at a centre-of-mass energy per nucleon pair $\sqrt{s_{NN}} = 5.02$ TeV with the ALICE experiment at the LHC. The D_s^+ mesons and their charge conjugates were reconstructed from the hadronic decay channel $D_s^+ \rightarrow \phi\pi^+$, with $\phi \rightarrow K^-K^+$, in the $4 < p_T < 36$ GeV/ c and $2 < p_T < 24$ GeV/ c intervals for the 0–10% and 30–50% centrality classes, respectively. The measured yields of non-prompt D_s^+ mesons are compared to those of prompt D_s^+ and non-prompt D^0 mesons by calculating the ratios of the production yields in Pb–Pb collisions and the nuclear modification factor R_{AA} . The ratio between the R_{AA} of non-prompt D_s^+ and prompt D_s^+ mesons, and that between the R_{AA} of non-prompt D_s^+ and non-prompt D^0 mesons in central Pb–Pb collisions are found to be on average higher than unity in the $4 < p_T < 12$ GeV/ c interval with a statistical significance of about 1.6σ and 1.7σ , respectively. The measured R_{AA} ratios are compared with the predictions of theoretical models of heavy-quark transport in a hydrodynamically expanding QGP that incorporate hadronisation via quark recombination.

arXiv:2204.10386v2 [nucl-ex] 4 Oct 2023

*See Appendix A for the list of collaboration members

1 Introduction

A transition from ordinary nuclear matter to a colour-deconfined medium called quark–gluon plasma (QGP) is predicted to occur at a very high temperature and energy density by quantum chromodynamics (QCD) calculations on the lattice [1–3], and is supported by several measurements in ultrarelativistic heavy-ion collisions at the SPS, RHIC, and LHC [4–11]. In such collisions, charm and beauty quarks are mainly produced in hard scattering processes that occur before the formation of the QGP. Hence, they are effective probes of the entire system evolution. While the system undergoes a hydrodynamic expansion, they interact with the medium constituents via elastic [12–14] and inelastic [15, 16] scatterings. These interactions imply that charm and beauty quarks exchange energy and momentum with the medium constituents, causing high-momentum quarks to lose part of their energy while traversing the QGP. The in-medium energy loss is commonly studied via the measurement of the nuclear modification factor,

$$R_{AA}(p_T) = \frac{1}{\langle T_{AA} \rangle} \times \frac{dN_{AA}/dp_T}{d\sigma_{pp}/dp_T}, \quad (1)$$

where dN_{AA}/dp_T is the transverse-momentum (p_T) differential production yield in nucleus–nucleus collisions, $d\sigma_{pp}/dp_T$ the p_T -differential cross section in proton–proton (pp) collisions, and $\langle T_{AA} \rangle$ is the average of the nuclear overlap function [17]. Several measurements of charm and beauty hadrons in Pb–Pb [18–30] and Au–Au [31–33] collisions show a strong suppression of the production yield at intermediate and high p_T ($p_T > 4\text{--}5$ GeV/ c) in heavy-ion collisions compared to pp collisions, suggesting a substantial energy loss of heavy quarks in the QGP. The comparison of the R_{AA} of light, charm, and beauty hadrons indicates that the energy loss is sensitive to the colour charge and the parton mass. In particular, the R_{AA} of beauty hadrons is observed to be larger than that of charm hadrons [21, 24]. For $p_T > 5\text{--}6$ GeV/ c , where radiative processes are expected to dominate the energy loss, the smaller suppression is attributed mainly to the so-called “dead cone” effect [34, 35], which suppresses the gluon radiation at angles smaller than $\theta \approx m_Q/E_Q$, where m_Q is the mass of the quark and E_Q its energy.

Instead, low- p_T heavy quarks experience a “Brownian motion”, which consists of a diffusion process occurring via multiple elastic interactions with low-momentum transfer [36]. Owing to the larger mass, beauty quarks diffuse less than charm quarks and have a longer relaxation time, which is expected to be proportional to the quark mass. Measurements of the heavy-flavour hadron production and azimuthal anisotropies can be exploited to constrain the spatial diffusion coefficient D_s via the comparison with theoretical models based on the heavy-quark transport in a hydrodynamically expanding QGP [18, 37].

A precise description of the hadronisation process in the hot nuclear matter is crucial to understand the transport properties of the QGP [38]. The hadronisation mechanism of low and intermediate- p_T heavy quarks is expected to be sensitive to the presence of a colour-deconfined medium, which could enable hadron formation via quark recombination in addition to the vacuum-like fragmentation. This leads to an enhancement of the production yield of heavy-flavour hadrons with strange-quark content relative to those of non-strange hadrons in Pb–Pb collisions compared to pp collisions, caused by the abundant production of strange–antistrange quark pairs in the QGP [11, 39, 40]. Recent measurements of the production of prompt D_s^+ mesons, i.e. D_s^+ mesons originating from the charm-quark hadronisation or decays of excited charm-hadron states, by the STAR [41] and ALICE [19, 42] Collaborations suggest a relevant role of the recombination mechanism in the charm-quark hadronisation. Similar studies in the open-beauty sector, conducted by the CMS Collaboration via the measurement of the B_s^0 -meson production relative to that of B^+ mesons, show a hint of enhanced production of strange over non-strange mesons [26, 43]. However, no firm conclusions can be drawn within the current uncertainties. Complementary information about the heavy-quark hadronisation in presence of the medium is provided by the measurements of charm baryons and charmonia in heavy-ion collisions [20, 27, 44–47]. Recently, the production of heavy-flavour hadrons containing strange quarks was also investigated in high-multiplicity

pp collisions [48, 49], following the observation of an enhanced production of strange and multi-strange hadrons with increasing charged-particle multiplicity in the light-flavour sector [50].

In this Letter, the measurement of the production of D_s^+ mesons originating from beauty-hadron decays (non-prompt) is reported for central (0–10%) and semicentral (30–50%) Pb–Pb collisions at a centre-of-mass energy per nucleon pair $\sqrt{s_{NN}} = 5.02$ TeV. Non-prompt D_s^+ mesons provide information about the diffusion and the energy loss of beauty quarks in the QGP. In addition, together with the measurement of non-prompt D^0 mesons, they have the potential to reveal the beauty-quark hadronisation mechanisms in the QGP, since in pp collisions about 50% of non-prompt D_s^+ mesons are produced in B_s^0 decays [51, 52]. Therefore, the non-prompt D_s^+ p_T -differential production yield and R_{AA} are compared with those of prompt D_s^+ and non-prompt D^0 mesons, as well as with theoretical models based on beauty-quark transport in the QGP.

2 Experimental apparatus and analysis technique

The D_s^+ -mesons were reconstructed from their hadronic decays with the ALICE central barrel detectors, which cover the full azimuth in the pseudorapidity interval $|\eta| < 0.9$ and are embedded in a large solenoidal magnet providing a uniform 0.5 T magnetic field parallel to the beam direction. Charged-particle trajectories are reconstructed from their hits in the Inner Tracking System (ITS) [53] and the Time Projection Chamber (TPC) [54]. Particle identification (PID) is provided via the measurement of the specific ionisation energy loss dE/dx in the TPC and of the flight time of the particles from the interaction point to the Time-Of-Flight detector (TOF) [55]. The reconstruction of the interaction vertex and of the decay vertices of charm- and beauty-hadron decays relies on the precise determination of the track parameters in the vicinity of the interaction point provided by the ITS.

The data sample of Pb–Pb collisions used in the analysis was collected with the ALICE detector in 2018, during LHC Run 2. Three trigger classes were considered: minimum bias, central, and semicentral, all based on the signals in the two scintillator arrays of the V0 detector [56], which covers the full azimuth in the pseudorapidity intervals $-3.7 < \eta < -1.7$ (V0C) and $2.8 < \eta < 5.1$ (V0A). Background events due to the interaction of one of the beams with residual gas in the vacuum tube and other machine-induced backgrounds were rejected offline using the timing information provided by the V0 and the neutron Zero Degree Calorimeters (ZDC) [57]. Only events with a primary vertex reconstructed within ± 10 cm from the centre of the detector along the beam-line direction were considered in the analysis. Collisions were classified into centrality intervals, defined in terms of percentiles of the hadronic Pb–Pb cross section, based on the V0 signal amplitude as described in detail in Ref. [58]. The measurement of non-prompt D_s^+ -meson production was carried out for central (0–10%) and semicentral (30–50%) collisions. The number of events considered for the analysis is about 100×10^6 and 85×10^6 in the 0–10% and 30–50% centrality intervals, corresponding to integrated luminosities \mathcal{L}_{int} of $(130.5 \pm 0.5) \mu\text{b}^{-1}$ and $(55.5 \pm 0.2) \mu\text{b}^{-1}$, respectively [59]. The average values of the nuclear overlap function, $\langle T_{AA} \rangle$, for the considered central and semicentral event intervals were estimated via Glauber-model [60] simulations anchored to the V0 signal amplitude distribution, and are $(23.26 \pm 0.17) \text{mb}^{-1}$ and $(3.92 \pm 0.06) \text{mb}^{-1}$ [17, 59], respectively.

The D_s^+ mesons and their charge conjugates were reconstructed via the $D_s^+ \rightarrow \phi\pi^+ \rightarrow K^-K^+\pi^+$ decay channel with branching ratio $\text{BR} = (2.24 \pm 0.08)\%$ [51]. The analysis was based on the reconstruction of decay-vertex topologies displaced from the interaction vertex. For prompt mesons, the separation between the interaction point and the D_s^+ decay vertex is governed by the mean proper decay length $c\tau$ of D_s^+ mesons, which is about $151 \mu\text{m}$ [51]. The decay vertices of non-prompt D_s^+ mesons on average are more displaced than those of prompt D_s^+ mesons due to the large mean proper decay lengths of beauty hadrons ($c\tau \simeq 450 \mu\text{m}$ [51]). Therefore, by exploiting the selection of displaced decay-vertex topologies, it is possible to separate non-prompt D_s^+ mesons from the combinatorial background and from prompt

D_s^+ mesons.

D_s^+ -meson candidates were built combining triplets of tracks with the proper charge signs, each with $|\eta| < 0.8$, at least 70 (out of a maximum of 159) crossed TPC pad rows, a track fit quality $\chi^2/\text{ndf} < 1.25$ in the TPC (where ndf is the number of degrees of freedom involved in the track fit procedure), and a minimum of two (out of a maximum of six) hits in the ITS, with at least one in either of the two innermost layers, which provide the best pointing resolution. Moreover, at least 50 clusters available for particle identification in the TPC were required, and only tracks with p_T above 0.6 (0.4) GeV/ c were considered for central (semicentral) collisions. These track selection criteria limit the D_s^+ -meson acceptance in rapidity, which drops steeply to zero for $|y| > 0.5$ at low p_T and for $|y| > 0.8$ at $p_T > 5$ GeV/ c . Thus, only D_s^+ -meson candidates within a p_T -dependent fiducial acceptance region, $|y| < y_{\text{fid}}(p_T)$, were selected. The $y_{\text{fid}}(p_T)$ value was defined as a second-order polynomial function, increasing from 0.5 to 0.8 in the transverse-momentum range $0 < p_T < 5$ GeV/ c , and as a constant term, $y_{\text{fid}} = 0.8$, for $p_T > 5$ GeV/ c .

Similarly to other recent D-meson measurements by the ALICE Collaboration [19, 21, 52], Boosted Decision Trees (BDT) algorithms were employed to reduce the large combinatorial background and to separate the contribution of prompt and non-prompt D_s^+ mesons through a multiclass classification. In particular, the implementation of the BDT algorithm provided by the XGBoost [61, 62] library was used. Background samples for the BDT training were extracted from the sidebands of the candidate invariant mass distributions in the data, namely from the $1.72 < M(\text{KK}\pi) < 1.83$ GeV/ c^2 and $2.01 < M(\text{KK}\pi) < 2.12$ GeV/ c^2 regions. Applying these selections, candidates belonging to $D^+ \rightarrow K^- K^+ \pi^+$ decays are rejected. Signal samples of prompt and non-prompt D_s^+ mesons were obtained from Monte Carlo (MC) simulations. The MC samples were built by simulating Pb–Pb collisions with the HIJING 1.36 [63] event generator in order to describe the charged-particle multiplicity and detector occupancy. To enrich the sample of prompt and non-prompt D-meson signals, additional $c\bar{c}$ - and $b\bar{b}$ -quark pairs were injected into each HIJING event using the PYTHIA 8.243 event generator [64, 65] with Monash tune [66]. The D_s^+ mesons were forced to decay into the hadronic channel of interest for the analysis. The generated particles were then propagated through the apparatus using the GEANT3 transport code [67]. Detailed descriptions of the detector response, the geometry of the apparatus and the conditions of the luminous region, including their evolution with time during the data taking period, were included in the simulation. Before the BDT training, loose kinematic and topological selections were applied to the D_s^+ -meson candidates together with the particle identification of decay-product tracks. The D_s^+ -meson candidate information provided to the BDTs, as an input for the models to distinguish among prompt and non-prompt mesons and background candidates, was mainly based on the displacement of the tracks from the primary vertex, the distance between the D_s^+ -meson decay vertex and the primary vertex, the D_s^+ -meson impact parameter, and the cosine of the pointing angle between the D_s^+ -meson candidate line of flight (the vector connecting the primary and secondary vertices) and its reconstructed momentum vector. In addition, the absolute difference between the reconstructed $K^+ K^-$ invariant mass and the PDG average mass for the ϕ meson [51] and variables related to the PID of decay tracks were also included. Independent BDTs were trained in the different p_T intervals of the analysis and for the different centrality intervals. Subsequently, they were applied to the real data sample in which the type of candidate is unknown. The BDT outputs are related to the candidate probability to be a non-prompt D_s^+ meson or combinatorial background. Selections on the BDT outputs were optimised to obtain a high non-prompt D_s^+ -meson fraction while maintaining a reliable signal extraction from the candidate invariant mass distributions.

The D_s^+ -meson candidates were selected by requiring a high probability to be non-prompt D_s^+ mesons and a low probability to be combinatorial background. The raw yield of D_s^+ mesons, including both particles and antiparticles, was extracted from binned maximum-likelihood fits to the invariant mass (M) distributions in transverse-momentum intervals $4 < p_T < 36$ GeV/ c and $2 < p_T < 24$ GeV/ c for the 0–10% and the 30–50% centrality intervals, respectively. The fit function was composed of a

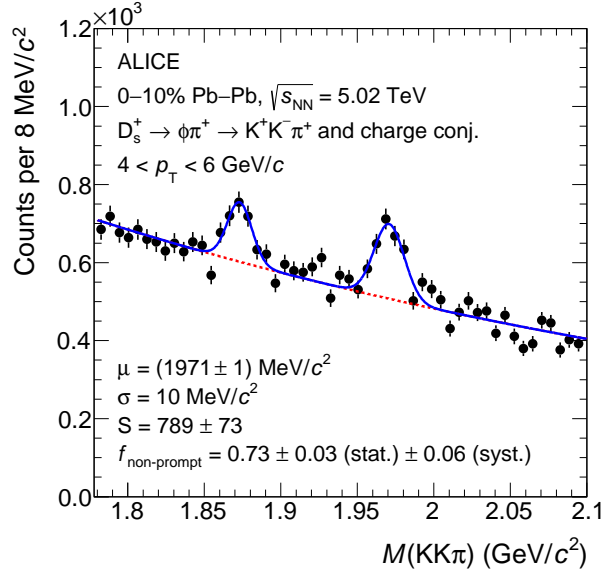


Figure 1: Invariant mass distribution of non-prompt D_s^+ candidates and their charge conjugates in the $4 < p_T < 6$ GeV/ c interval for central Pb–Pb collisions. The blue solid line shows the total fit function and the red dashed line the combinatorial-background contribution. The values of the mean (μ), width (σ), and raw yield (S) of the signal peak are reported together with their statistical uncertainties resulting from the fit. The fraction of non-prompt candidates in the measured raw yield is reported with its statistical and systematic uncertainties.

Gaussian for the description of the signal and an exponential term for the background. An additional Gaussian was used to describe the peak due to the decay $D^+ \rightarrow K^- K^+ \pi^+$, with a branching ratio of $(9.68 \pm 0.18) \times 10^{-3}$ [51], present at a lower invariant mass value than the D_s^+ -meson signal peak. To improve the stability of the fits, the width of the D_s^+ -meson signal peak was fixed to the value extracted from a data sample dominated by prompt candidates, which is characterised by a signal extraction with higher statistical significance. As an example, the invariant mass distribution for the $4 < p_T < 6$ GeV/ c interval in central Pb–Pb collisions, together with the result of the fit and the estimated non-prompt fraction is reported in Fig. 1. The measured raw yield, although dominated by non-prompt candidates, still contains a residual contribution of prompt D_s^+ mesons which satisfy the BDT-based selections. The procedure used to calculate the fraction of non-prompt candidates present in the extracted raw yield is described below. The statistical significance of the observed signals varies from about 4 to 11 depending upon the p_T and centrality intervals.

The corrected p_T -differential yields of non-prompt D_s^+ mesons were computed for each p_T interval as

$$\left. \frac{dN}{dp_T} \right|_{|y| < 0.5} = \frac{1}{2} \times \frac{1}{\Delta p_T} \times \frac{f_{\text{non-prompt}}(p_T) \times N^{\text{D}^+ \bar{\text{D}}^+, \text{raw}}(p_T) \Big|_{|y| < y_{\text{fid}}(p_T)}}{c_{\Delta y}(p_T) \times (\text{Acc} \times \varepsilon)_{\text{non-prompt}}(p_T) \times \text{BR} \times N_{\text{evt}}}. \quad (2)$$

The raw-yield values $N^{\text{D}^+ \bar{\text{D}}^+, \text{raw}}$ were divided by a factor of two and multiplied by the non-prompt fraction $f_{\text{non-prompt}}$ to obtain the charge-averaged yields of non-prompt D_s^+ mesons. Furthermore, they were divided by the acceptance-times-efficiency correction factor of non-prompt D_s^+ mesons $(\text{Acc} \times \varepsilon)_{\text{non-prompt}}$, the BR of the decay channel, the width of the p_T interval Δp_T , the correction factor for the rapidity coverage $c_{\Delta y}$, and the number of analysed events N_{evt} . The correction factor for the rapidity acceptance $c_{\Delta y}$ was defined as the ratio between the generated D-meson yield in $\Delta y = 2 y_{\text{fid}}(p_T)$ and that in $|y| < 0.5$. It was computed with FONLL perturbative QCD calculations [68, 69] as in Refs. [18, 19].

The $(\text{Acc} \times \varepsilon)$ correction factor was obtained from MC simulations, using samples not employed in the BDT training. The D_s^+ -meson p_T distributions from simulations were reweighed in order to mimic the

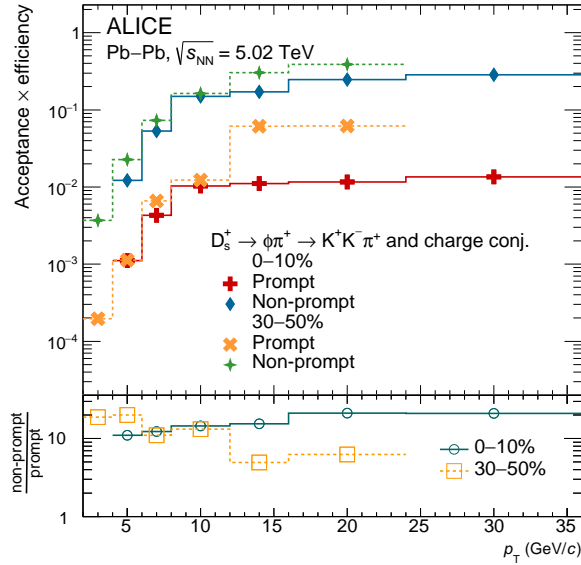


Figure 2: Acceptance-times-efficiency factors for prompt and non-prompt D_s^+ mesons as a function of p_T in the 0–10% and 30–50% centrality intervals, together with their ratios (bottom panel).

realistic shapes in the determination of the $(\text{Acc} \times \varepsilon)$ factor, which depends on p_T . In particular, weights were applied to the p_T distributions of prompt D_s^+ mesons and of beauty-hadron mother particles in case of non-prompt D_s^+ mesons. These weights were defined to reproduce the shapes given by FONLL calculations multiplied by the R_{AA} of prompt D_s^+ mesons and B mesons predicted by the TAMU [70, 71] model. The TAMU model implements the charm- and beauty-quark transport inside a strangeness-rich QGP, and it reasonably reproduces the prompt D-meson measurements at low p_T [18, 19]. The $(\text{Acc} \times \varepsilon)$ factors as a function of p_T for prompt and non-prompt D_s^+ mesons in the 0–10% and 30–50% centrality intervals are displayed in Fig. 2, along with the ratios of the non-prompt to prompt factors. The prompt D_s^+ -meson acceptance times efficiency is smaller than that of non-prompt D_s^+ mesons by a factor varying from 5 to 20 depending on p_T and centrality. This is expected since the selections applied to obtain the non-prompt enriched sample strongly suppress the prompt D_s^+ -meson efficiency. Instead, the acceptance is the same for prompt and non-prompt mesons. In central collisions, the prompt D_s^+ -meson suppression increases with increasing p_T . The opposite trend is observed in semicentral collisions, since less stringent selections on the BDT outputs are necessary to extract the non-prompt D_s^+ -meson signal due to the lower yield.

The fraction $f_{\text{non-prompt}}$ of non-prompt D_s^+ mesons in the extracted raw yield was estimated with a data-driven procedure based on the construction of data samples with different abundances of prompt and non-prompt candidates. These samples were built by varying the selection on the BDT output related to the candidate probability to be a non-prompt D_s^+ meson. Starting from the values of raw yield and acceptance times efficiency of prompt and non-prompt D_s^+ mesons obtained for each sample, the corrected yield of prompt and non-prompt D_s^+ mesons and the $f_{\text{non-prompt}}$ fraction were calculated. This data-driven technique does not depend on theoretical calculations of heavy-quark production and interaction with the QGP constituents, and it is described in detail in Ref. [52]. The $f_{\text{non-prompt}}$ fractions obtained as a function of p_T in central and semicentral Pb–Pb collisions are reported in Fig. 3, together with their statistical and systematic uncertainties. The determination of the systematic uncertainty on the $f_{\text{non-prompt}}$ fraction is described in Section 3. The $f_{\text{non-prompt}}$ values vary between about 0.72 (0.56) and 0.82 (0.70) in the 0–10% (30–50%) centrality interval as a function of transverse momentum. The $f_{\text{non-prompt}}$ is observed to be on average lower in semicentral collision with respect to central collisions. This difference is expected as in the 30–50% centrality interval less stringent BDT selections were applied compared to

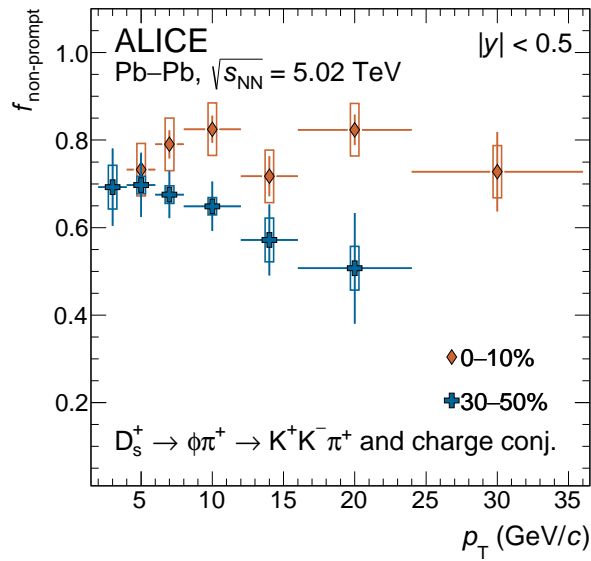


Figure 3: Fraction of non-prompt D_s^+ mesons in the extracted raw yield as a function of p_T in the 0–10% and 30–50% centrality intervals. The vertical bars (boxes) report the statistical (systematic) uncertainties.

0–10% centrality interval.

The non-prompt D_s^+ -meson nuclear modification factor, R_{AA} , was computed according to Eq. 1. The measurement of the p_T -differential cross section of non-prompt D_s^+ mesons at midrapidity ($|y| < 0.5$) in pp collisions at $\sqrt{s} = 5.02$ TeV from Ref. [52], which covers the transverse-momentum interval $2 < p_T < 12$ GeV/c, was used as the reference for the R_{AA} computation. For $p_T > 12$ GeV/c, an extrapolated pp reference was obtained from FONLL calculations of the beauty-hadron cross section and by using PYTHIA 8 to describe the decay kinematics of beauty hadrons to D_s^+ mesons, for more details see Ref. [52]. The resulting predictions were then scaled to match the measured values at lower transverse momenta. The total systematic uncertainty on the pp reference is $^{+38}_{-28}\%$ for all the extrapolated p_T intervals. The procedures for the p_T extrapolation and the systematic uncertainty estimation are the same as in Ref. [72].

3 Systematic uncertainties

The following sources of systematic uncertainty were considered for the production yield and R_{AA} estimation: (i) the raw-yield extraction, (ii) track reconstruction efficiency, (iii) non-prompt D_s^+ -meson fraction, (iv) BDT selection efficiency, (v) PID selection efficiency, (vi) relative abundances of beauty-hadron species in the MC simulation, and (vii) shapes of the simulated p_T -differential distributions. The resulting systematic uncertainties on the non-prompt D_s^+ -meson yield and R_{AA} in representative p_T intervals are summarised in Table 1. In the R_{AA} computation, the systematic uncertainties on the pp measurement were treated as uncorrelated from the ones on the Pb–Pb corrected yields, except for the uncertainty on the BR (3.6%) [51] which cancels in the R_{AA} and was considered only in the p_T -differential production yield. The normalisation uncertainty on the R_{AA} includes the uncertainty on the integrated luminosity in pp collisions (2.1% [73]), the uncertainty on the $\langle T_{AA} \rangle$ estimation, 0.7% (1.5%) for the 0–10% (30–50%) centrality interval [17], and the one related to the centrality-interval definition. This last contribution is due to the uncertainty on the fraction of the hadronic cross section used in the Glauber fit to determine the centrality. It was estimated to be $< 0.1\%$ and 2% for the 0–10% and 30–50% centrality intervals, respectively [72].

The systematic uncertainty on the raw-yield extraction was estimated by adopting several fit configu-

rations changing the background fit function (linear and parabolic), the upper and lower fit limits, and the bin size of the invariant mass spectrum. The sensitivity to the line shape of the D_s^+ peak was tested by comparing the raw-yield values from the fits with those obtained by counting the candidates in the invariant mass region of the signal after subtracting the background estimated from the side bands.

The systematic uncertainty on the track reconstruction efficiency accounts for possible discrepancies between data and MC in the ITS–TPC prolongation efficiency and in the selection efficiency due to track-quality criteria in the TPC. The per-track systematic uncertainties were estimated by varying the track-quality selection criteria and by comparing the prolongation probability of the TPC tracks to the ITS hits in data and simulations. They were then propagated to the non-prompt D_s^+ mesons via their decay kinematics.

The systematic uncertainties on the non-prompt D_s^+ -meson fraction and the BDT selection efficiency are due to possible discrepancies between data and MC in the distributions of the variables used in the BDT-model training (i.e. the D_s^+ -meson decay-vertex topology, kinematic, and PID variables). The former was computed by varying the configuration and the number of BDT selections employed in the data-driven method described in Sec. 2. In particular, wider and narrower intervals of the probability to be non-prompt D_s^+ mesons, and smaller and larger step sizes between the chosen BDT selections were considered. For each configuration, the non-prompt D_s^+ -meson fraction was recomputed. The systematic uncertainty related to the BDT selection efficiency was studied by repeating the entire analysis varying the selection criteria based on the BDT outputs. The uncertainty for this source of systematic uncertainty was assigned considering the RMS and the shift of the corrected yield obtained by varying the BDT selection with respect to the reference one.

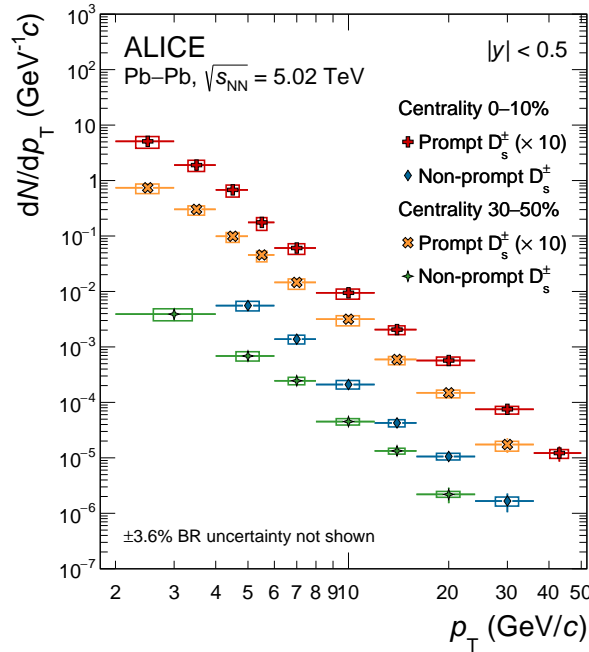
Analogously, the systematic uncertainty on the PID selection efficiency relative to the loose selection on the PID variables applied before the BDT ones was also considered. This source was evaluated in the prompt D_s^+ -meson analysis [19], and it was found to be negligible for the adopted PID strategy.

The selection efficiency of non-prompt D_s^+ mesons originating from the decay of different beauty-hadron species can differ because of the different lifetime of the parent hadron and the different decay kinematics. Consequently, an imperfect description in the MC simulation of the beauty-hadron composition might result in a bias in the estimation of the D-meson efficiencies. This is especially important for D_s^+ mesons, which receive significant contributions from all the three ground-state B-meson species (B^+ , B^0 , and B_s^0). The PYTHIA 8 event generator describes the measurements of different B-meson species in pp collisions [52], however in heavy-ion collisions an enhanced production of strange over non-strange B mesons is expected compared to the one observed in pp collisions. Nevertheless, since no precise measurement of B_s^0 -meson production down to low momentum is available in Pb–Pb collisions, the relative abundances present in PYTHIA 8 were used without applying any reweighting. The systematic uncertainty introduced by this assumption was estimated by reweighting the B_s^0 contribution present in the MC enhanced by a factor 2 as predicted by the TAMU model [70]. The systematic uncertainty was assigned considering the variation between the production yield estimated using the enhanced B_s^0 contribution and the default one.

The systematic uncertainty due to the shape of the p_T distributions of D_s^+ mesons and beauty hadrons in the MC simulations was evaluated by applying different weights to the p_T distributions of prompt D_s^+ mesons and of beauty-hadron mother particles in case of non-prompt D_s^+ mesons. As an alternative to the TAMU model, the shape resulting from the LIDO model [74] was considered. The main difference between the TAMU and LIDO model derives from the fact that the former includes the enhanced production of the B_s^0 mesons, unlike the latter. An additional variation of the shape of the p_T distributions of prompt D_s^+ mesons was included considering the results from Ref. [19]. The systematic uncertainty was assigned considering the variation of the corrected yield compared to the default case.

Table 1: Systematic uncertainties on the measurement of the non-prompt D_s^+ -meson corrected yield and R_{AA} in the 0–10% and 30–50% centrality intervals for representative transverse-momentum intervals.

Centrality interval p_T (GeV/ c)	0–10%		30–50%	
	4–6	12–16	2–4	12–16
Yield extraction	5%	5%	10%	5%
Tracking efficiency	13%	13%	11%	12%
Non-prompt fraction	6%	6%	5%	6%
Selection efficiency	8%	5%	10%	5%
PID efficiency	negl.	negl.	negl.	negl.
B hadrochemistry	1%	1%	1%	1%
MC p_T shape	10%	8%	15%	2%
Centrality limits	< 0.1%		2%	
$\langle T_{AA} \rangle$	0.7%		1.5%	
\mathcal{L}_{int}^{pp}			2.1%	
Branching ratio			3.6%	

**Figure 4:** Prompt and non-prompt D_s^+ meson production yield in central and semicentral Pb–Pb collisions at $\sqrt{s_{NN}} = 5.02$ TeV. The prompt D_s^+ results are taken from Ref. [19] and scaled by a factor 10 for visibility. The vertical bars (boxes) report the statistical (systematic) uncertainties.

4 Results

Figure 4 shows the p_T -differential production yield of prompt and non-prompt D_s^+ mesons in central and semicentral Pb–Pb collisions at $\sqrt{s_{NN}} = 5.02$ TeV. The measured prompt D_s^+ -meson production yields were taken from Ref. [19] and scaled by a factor 10 for visibility.

Figure 5 reports the ratios of the production yield of non-prompt to prompt D_s^+ (left panel) and non-prompt D_s^+ to non-prompt D^0 [21] (right panel) in central and semicentral Pb–Pb collisions, as well as in pp collisions [52]. Computing these ratios helps to further investigate the effects of the QGP medium on

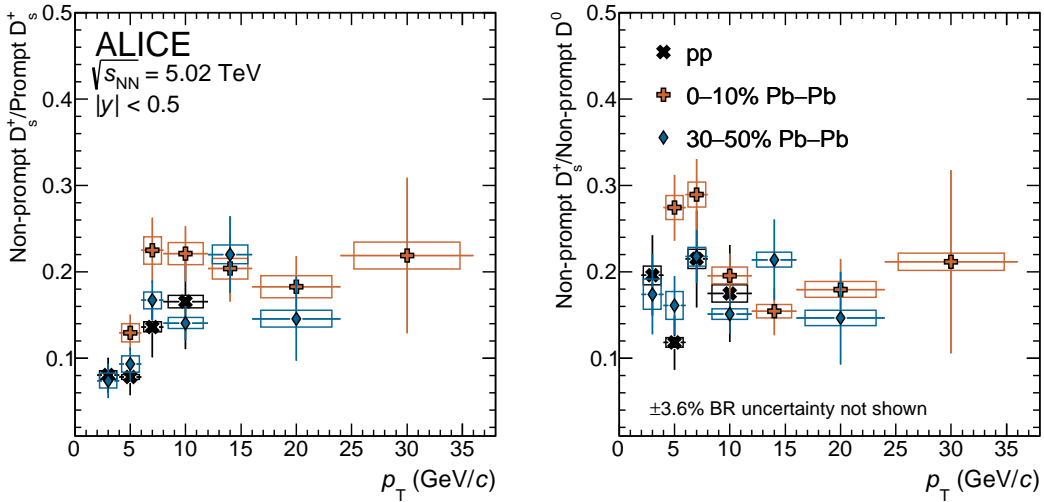


Figure 5: The p_T -differential production yield of non-prompt D_s^+ mesons divided by those of prompt D_s^+ mesons (left panel) and non-prompt D^0 mesons (right panel) for the 0–10% and 30–50% centrality intervals in Pb–Pb collisions at $\sqrt{s_{NN}} = 5.02$ TeV from Refs. [19, 21] compared with those in pp collisions at the same centre-of-mass energy from Ref. [52].

the hadron formation mechanism. To get an indication of the B_s^0 -meson p_T probed by non-prompt D_s^+ mesons, a simulation with PYTHIA 8 was performed. As an example, the mean p_T distribution of B_s^0 mesons decaying to D_s^+ mesons with $4 < p_T < 6$ GeV/c has a mean of about 8.8 GeV/c and an RMS of about 3.1 GeV/c. The non-prompt to prompt D_s^+ -meson ratio ranges between about 0.05 and 0.20 and increases with increasing p_T up to $p_T = 10$ GeV/c. At higher momentum the slope of the ratios seems to reduce, even though no firm conclusions can be drawn with the current uncertainties. On the other hand, the non-prompt D_s^+ to non-prompt D^0 ratio shows an almost flat trend around 0.2 in the p_T range of the measurement. The ratios computed in pp and semicentral Pb–Pb collisions are compatible within the uncertainties. A hint of enhancement compared to pp collisions with a significance of 1.7σ , where σ indicates the sum in quadrature of statistical and systematic uncertainties, is found by performing a weighted average of the non-prompt D_s^+/D^0 values in the $4 < p_T < 12$ GeV/c interval for the 0–10% centrality class. The inverse of the squared sum of the relative statistical and p_T -uncorrelated systematic uncertainties was used as weight in the average. All the systematic uncertainties, except for those on the raw-yield extraction, were considered as fully correlated in p_T . This hint of a larger non-prompt D_s^+/D^0 yield ratio is consistent with an enhanced production of strange-beauty mesons in heavy-ion collisions compared to pp collisions, as expected in a scenario in which beauty quarks hadronise via recombination with surrounding quarks in the strangeness-enriched QGP medium. In the transverse-momentum interval $4 < p_T < 12$ GeV/c, also the non-prompt to prompt D_s^+ -meson ratio in the 0–10% centrality class shows a mild enhancement with respect to pp collisions with a significance of 1.6σ .

The R_{AA} of non-prompt D_s^+ mesons was computed according to Eq. 1, where the pp reference was obtained from the measurement published in Ref. [52]. To study the effects of the QGP medium on the resulting momentum spectra and the hadronisation mechanism of beauty quarks, the nuclear modification factor measured for the non-prompt D_s^+ mesons was compared to that of prompt D_s^+ [19] and non-prompt D^0 [21] mesons measured at the same centre-of-mass energy per nucleon pair. The prompt and non-prompt D_s^+ R_{AA} are compared in the top- and bottom-left panels of Fig. 6 for the 0–10% and 30–50% centrality class, respectively. Analogously, the comparison between the nuclear modification factor of non-prompt D_s^+ and non-prompt D^0 mesons is reported in the right panels of the same figure. The R_{AA} of prompt and non-prompt D mesons shows a decreasing trend with increasing p_T up to a minimum of about 0.2 (0.4) around 10 GeV/c in the 0–10% (30–50%) centrality class. In the lowest p_T intervals,

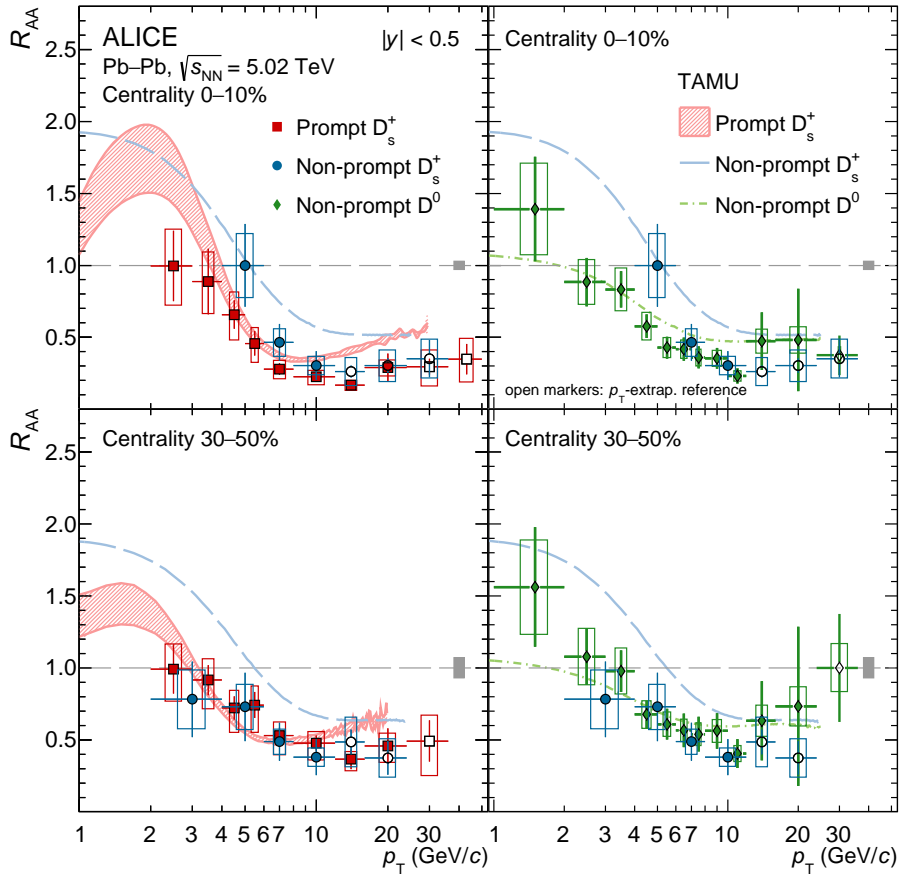


Figure 6: Left panels: prompt (Ref. [19]) and non-prompt D_s^+ -meson R_{AA} in central (top) and semicentral (bottom) Pb–Pb collisions at $\sqrt{s_{NN}} = 5.02$ TeV. Right panels: non-prompt D_s^+ - and D^0 -meson (Ref. [21]) R_{AA} in central (top) and semicentral (bottom) Pb–Pb collisions at $\sqrt{s_{NN}} = 5.02$ TeV. The experimental results are compared with the predictions of the TAMU model [70]. Statistical (bars), systematic (boxes), and normalisation (shaded box around unity) uncertainties are shown.

the R_{AA} increases up to unity. In particular, the central values of the non-prompt D_s^+ R_{AA} are higher with respect to those of prompt D_s^+ and non-prompt D^0 in the 0–10% centrality class for $p_T < 6$ GeV/c, even though they are compatible within uncertainties. This possible difference between prompt and non-prompt D_s^+ R_{AA} would be consistent with the different loss of energy experienced by charm and beauty quarks traversing the QGP. In fact, the effect due to the different decay kinematics of charm and beauty hadrons is found to be negligible, as discussed in Ref. [21]. Instead, the difference between non-prompt D_s^+ and D^0 mesons could result from the hadronisation via recombination and the presence of a strangeness-rich environment. In semicentral collisions, no separation among the R_{AA} of prompt D_s^+ , non-prompt D_s^+ , and non-prompt D^0 is observed within the measurement uncertainties.

The R_{AA} measurements were compared with the predictions of the TAMU model [70]. In the TAMU model, the heavy-quark transport is described via the Langevin equation and the hadronisation can occur both via recombination with light quarks from the medium, which is the dominant mechanism at low p_T , or via fragmentation, which becomes more important at high p_T . The TAMU predictions are shown in Fig. 6. The uncertainty band for prompt D_s^+ mesons is due to the modification of the parton distribution functions in Pb nuclei, which is neglected for the beauty-quark production. The TAMU model qualitatively describes the p_T trend of the non-prompt D_s^+ -meson R_{AA} , although it overestimates the measurements.

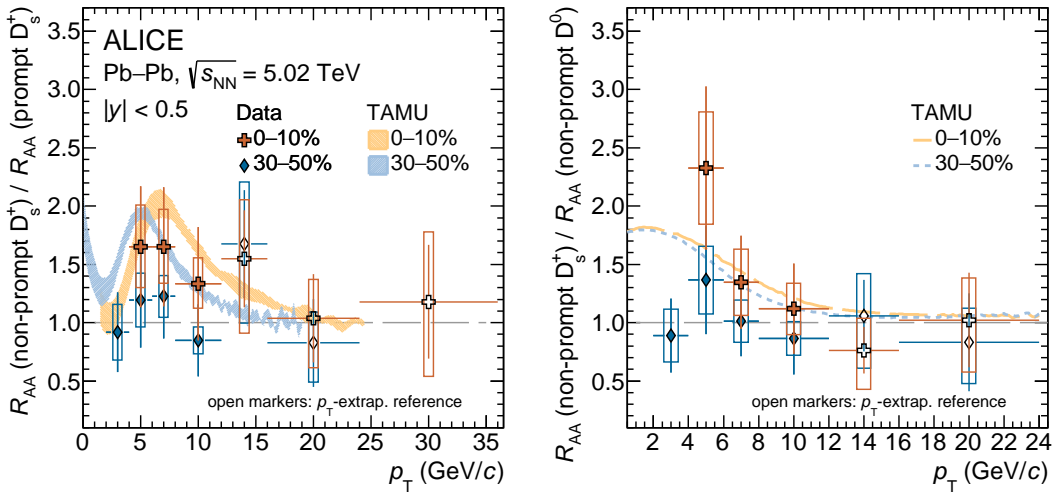


Figure 7: The R_{AA} of non-prompt D_s^+ mesons divided by the one of prompt D_s^+ mesons [19] (left panel) and non-prompt D^0 mesons [21] (right panel) for the 0–10% and 30–50% centrality intervals in Pb–Pb collisions at $\sqrt{s_{NN}} = 5.02$ TeV. The measurements are compared with TAMU model predictions [70]. Statistical (bars) and systematic (boxes) uncertainties are shown.

In the left and right panels of Fig. 7, the nuclear modification factors of non-prompt D_s^+ mesons divided by that of prompt D_s^+ mesons and non-prompt D^0 mesons are shown, respectively. The measurements in both centrality intervals are compared with the predictions of the TAMU model. In the 0–10% centrality class, the non-prompt D_s^+ to prompt D_s^+ R_{AA} ratio suggests a hint of enhancement with a statistical significance of 1.6σ in the $4 < p_T < 12$ GeV/ c interval, which is by construction the same of that reported for the corresponding yield ratio. The R_{AA} ratio is consistent with a larger energy loss for the charm quark with respect to the beauty quark due to its smaller mass, as already suggested by the results shown in Fig. 6. No hint for a ratio of the R_{AA} larger than unity is observed in semicentral collisions. Considering the measurement uncertainties, TAMU predictions qualitatively describe the results for central collisions. At variance, for semicentral collisions the TAMU model overestimates the R_{AA} ratio values. The measurements of the non-prompt D_s^+ to non-prompt D^0 R_{AA} ratio suggest a possible enhancement with respect to unity in the $4 < p_T < 12$ GeV/ c interval for central collisions, as reported for the yield ratio. In this case, the rise at low p_T might be a consequence of the abundance of strange quarks thermally produced in the QGP and the dominance of the hadronisation via recombination in this range of momentum. The TAMU model describes the data within the experimental uncertainties.

5 Conclusions

In this Letter, the first measurement of the non-prompt D_s^+ -meson production at midrapidity in Pb–Pb collisions at $\sqrt{s_{NN}} = 5.02$ TeV was reported.

The non-prompt D_s^+ -meson production yield was measured between 4 and 36 (2 and 24) GeV/ c in the 0–10% (30–50%) centrality interval. These measurements were compared to the ones performed for prompt D_s^+ and non-prompt D^0 mesons at the same centre-of-mass energy. The production yield was employed to compute the non-prompt D_s^+ -meson R_{AA} , which was compared with the R_{AA} of prompt D_s^+ and non-prompt D^0 mesons.

The non-prompt D_s^+ R_{AA} shows a significant p_T dependence. A minimum at intermediate transverse momentum ($p_T \approx 10$ GeV/ c) around 0.2 (0.4) in central (semicentral) collisions, and a mild increase with decreasing p_T , with R_{AA} reaching (close to) unity at $p_T \approx 4$ –6 (2–4) GeV/ c in the 0–10% (30–

50%) centrality interval are reported. The TAMU model, which implements the parton in-medium energy loss through collisional processes as well as the beauty-quark hadronisation both via fragmentation and recombination, describes the p_T trend of the R_{AA} . However, it overestimates the measurements. Further comparisons were performed between prompt and non-prompt D_s^+ as well as non-prompt D^0 mesons by computing the ratios of their production yields and R_{AA} . These ratios suggest the presence of an enhancement of non-prompt D_s^+ mesons compared to prompt D_s^+ (non-prompt D^0) mesons in central collisions in the $4 < p_T < 12$ GeV/ c interval, with a significance of 1.6σ (1.7σ). The increase is consistent with expectations for the overall effect of the energy-loss mechanism and the hadronisation-process modification in presence of the colour-deconfined medium.

The recent upgrade of the ALICE apparatus will greatly enhance the physics potential of the experiment in the LHC Run 3 data-taking period, allowing for more precise measurements of the non-prompt D_s^+ -meson production in heavy-ion collisions.

Acknowledgements

The ALICE Collaboration would like to thank all its engineers and technicians for their invaluable contributions to the construction of the experiment and the CERN accelerator teams for the outstanding performance of the LHC complex. The ALICE Collaboration gratefully acknowledges the resources and support provided by all Grid centres and the Worldwide LHC Computing Grid (WLCG) collaboration. The ALICE Collaboration acknowledges the following funding agencies for their support in building and running the ALICE detector: A. I. Alikhanyan National Science Laboratory (Yerevan Physics Institute) Foundation (ANSL), State Committee of Science and World Federation of Scientists (WFS), Armenia; Austrian Academy of Sciences, Austrian Science Fund (FWF): [M 2467-N36] and Nationalstiftung für Forschung, Technologie und Entwicklung, Austria; Ministry of Communications and High Technologies, National Nuclear Research Center, Azerbaijan; Conselho Nacional de Desenvolvimento Científico e Tecnológico (CNPq), Financiadora de Estudos e Projetos (Finep), Fundação de Amparo à Pesquisa do Estado de São Paulo (FAPESP) and Universidade Federal do Rio Grande do Sul (UFRGS), Brazil; Bulgarian Ministry of Education and Science, within the National Roadmap for Research Infrastructures 2020-2027 (object CERN), Bulgaria; Ministry of Education of China (MOEC), Ministry of Science & Technology of China (MSTC) and National Natural Science Foundation of China (NSFC), China; Ministry of Science and Education and Croatian Science Foundation, Croatia; Centro de Aplicaciones Tecnológicas y Desarrollo Nuclear (CEADEN), Cubaenergía, Cuba; Ministry of Education, Youth and Sports of the Czech Republic, Czech Republic; The Danish Council for Independent Research | Natural Sciences, the VILLUM FONDEN and Danish National Research Foundation (DNRF), Denmark; Helsinki Institute of Physics (HIP), Finland; Commissariat à l’Energie Atomique (CEA) and Institut National de Physique Nucléaire et de Physique des Particules (IN2P3) and Centre National de la Recherche Scientifique (CNRS), France; Bundesministerium für Bildung und Forschung (BMBF) and GSI Helmholtzzentrum für Schwerionenforschung GmbH, Germany; General Secretariat for Research and Technology, Ministry of Education, Research and Religions, Greece; National Research, Development and Innovation Office, Hungary; Department of Atomic Energy Government of India (DAE), Department of Science and Technology, Government of India (DST), University Grants Commission, Government of India (UGC) and Council of Scientific and Industrial Research (CSIR), India; National Research and Innovation Agency - BRIN, Indonesia; Istituto Nazionale di Fisica Nucleare (INFN), Italy; Japanese Ministry of Education, Culture, Sports, Science and Technology (MEXT) and Japan Society for the Promotion of Science (JSPS) KAKENHI, Japan; Consejo Nacional de Ciencia (CONACYT) y Tecnología, through Fondo de Cooperación Internacional en Ciencia y Tecnología (FONCICYT) and Dirección General de Asuntos del Personal Académico (DGAPA), Mexico; Nederlandse Organisatie voor Wetenschappelijk Onderzoek (NWO), Netherlands; The Research Council of Norway, Norway; Commission on Science and Technology for Sustainable Development in the South (COMSATS), Pakistan;

Pontificia Universidad Católica del Perú, Peru; Ministry of Education and Science, National Science Centre and WUT ID-UB, Poland; Korea Institute of Science and Technology Information and National Research Foundation of Korea (NRF), Republic of Korea; Ministry of Education and Scientific Research, Institute of Atomic Physics, Ministry of Research and Innovation and Institute of Atomic Physics and University Politehnica of Bucharest, Romania; Ministry of Education, Science, Research and Sport of the Slovak Republic, Slovakia; National Research Foundation of South Africa, South Africa; Swedish Research Council (VR) and Knut & Alice Wallenberg Foundation (KAW), Sweden; European Organization for Nuclear Research, Switzerland; Suranaree University of Technology (SUT), National Science and Technology Development Agency (NSTDA) and National Science, Research and Innovation Fund (NSRF via PMU-B B05F650021), Thailand; Turkish Energy, Nuclear and Mineral Research Agency (TENMAK), Turkey; National Academy of Sciences of Ukraine, Ukraine; Science and Technology Facilities Council (STFC), United Kingdom; National Science Foundation of the United States of America (NSF) and United States Department of Energy, Office of Nuclear Physics (DOE NP), United States of America. In addition, individual groups or members have received support from: Marie Skłodowska Curie, Strong 2020 - Horizon 2020, European Research Council (grant nos. 824093, 896850, 950692), European Union; Academy of Finland (Center of Excellence in Quark Matter) (grant nos. 346327, 346328), Finland; Programa de Apoyos para la Superación del Personal Académico, UNAM, Mexico.

References

- [1] F. Karsch, “Lattice simulations of the thermodynamics of strongly interacting elementary particles and the exploration of new phases of matter in relativistic heavy ion collisions”, *J. Phys. Conf. Ser.* **46** (2006) 122–131, arXiv:hep-lat/0608003.
- [2] S. Borsanyi, Z. Fodor, J. N. Guenther, R. Kara, S. D. Katz, P. Parotto, A. Pasztor, C. Ratti, and K. K. Szabo, “QCD Crossover at Finite Chemical Potential from Lattice Simulations”, *Phys. Rev. Lett.* **125** (2020) 052001, arXiv:2002.02821 [hep-lat].
- [3] **HotQCD** Collaboration, A. Bazavov *et al.*, “Chiral crossover in QCD at zero and non-zero chemical potentials”, *Phys. Lett. B* **795** (2019) 15–21, arXiv:1812.08235 [hep-lat].
- [4] U. W. Heinz and M. Jacob, “Evidence for a new state of matter: An Assessment of the results from the CERN lead beam program”, arXiv:nucl-th/0002042.
- [5] **BRAHMS** Collaboration, I. Arsene *et al.*, “Quark gluon plasma and color glass condensate at RHIC? The Perspective from the BRAHMS experiment”, *Nucl. Phys. A* **757** (2005) 1–27, arXiv:nucl-ex/0410020.
- [6] **PHOBOS** Collaboration, B. B. Back *et al.*, “The PHOBOS perspective on discoveries at RHIC”, *Nucl. Phys. A* **757** (2005) 28–101, arXiv:nucl-ex/0410022.
- [7] **STAR** Collaboration, J. Adams *et al.*, “Experimental and theoretical challenges in the search for the quark gluon plasma: The STAR Collaboration’s critical assessment of the evidence from RHIC collisions”, *Nucl. Phys. A* **757** (2005) 102–183, arXiv:nucl-ex/0501009.
- [8] **PHENIX** Collaboration, K. Adcox *et al.*, “Formation of dense partonic matter in relativistic nucleus-nucleus collisions at RHIC: Experimental evaluation by the PHENIX collaboration”, *Nucl. Phys. A* **757** (2005) 184–283, arXiv:nucl-ex/0410003.
- [9] **ALICE** Collaboration, S. Acharya *et al.*, “Transverse momentum spectra and nuclear modification factors of charged particles in pp, p-Pb and Pb-Pb collisions at the LHC”, *JHEP* **11** (2018) 013, arXiv:1802.09145 [nucl-ex].

- [10] ALICE Collaboration, J. Adam *et al.*, “Anisotropic flow of charged particles in Pb–Pb collisions at $\sqrt{s_{NN}} = 5.02$ TeV”, *Phys. Rev. Lett.* **116** (2016) 132302, arXiv:1602.01119 [nucl-ex].
- [11] P. Braun-Munzinger, V. Koch, T. Schäfer, and J. Stachel, “Properties of hot and dense matter from relativistic heavy ion collisions”, *Phys. Rept.* **621** (2016) 76–126, arXiv:1510.00442 [nucl-th].
- [12] M. H. Thoma and M. Gyulassy, “Quark Damping and Energy Loss in the High Temperature QCD”, *Nucl. Phys. B* **351** (1991) 491–506.
- [13] E. Braaten and M. H. Thoma, “Energy loss of a heavy fermion in a hot plasma”, *Phys. Rev. D* **44** (1991) 1298–1310.
- [14] E. Braaten and M. H. Thoma, “Energy loss of a heavy quark in the quark - gluon plasma”, *Phys. Rev. D* **44** (1991) R2625.
- [15] R. Baier, Y. L. Dokshitzer, A. H. Mueller, S. Peigné, and D. Schiff, “Radiative energy loss and p_T broadening of high-energy partons in nuclei”, *Nucl. Phys. B* **484** (1997) 265–282, arXiv:hep-ph/9608322.
- [16] M. Gyulassy and M. Plumer, “Jet Quenching in Dense Matter”, *Phys. Lett. B* **243** (1990) 432–438.
- [17] ALICE Collaboration, “Centrality determination in heavy ion collisions”, *ALICE-PUBLIC-2018-011* (Aug, 2018) . <https://cds.cern.ch/record/2636623>.
- [18] ALICE Collaboration, S. Acharya *et al.*, “Prompt D^0 , D^+ , and D^{*+} production in Pb–Pb collisions at $\sqrt{s_{NN}} = 5.02$ TeV”, *JHEP* **01** (2022) 174, arXiv:2110.09420 [nucl-ex].
- [19] ALICE Collaboration, S. Acharya *et al.*, “Measurement of prompt D_s^+ -meson production and azimuthal anisotropy in Pb–Pb collisions at $\sqrt{s_{NN}} = 5.02$ TeV”, *Phys. Lett. B* **827** (2022) 136986, arXiv:2110.10006 [nucl-ex].
- [20] ALICE Collaboration, S. Acharya *et al.*, “Constraining hadronization mechanisms with Λ_c^+/D^0 production ratios in Pb–Pb collisions at $\sqrt{s_{NN}} = 5.02$ TeV”, *Phys. Lett. B* **839** (2023) 137796, arXiv:2112.08156 [nucl-ex].
- [21] ALICE Collaboration, S. Acharya *et al.*, “Measurement of beauty production via non-prompt D^0 mesons in Pb–Pb collisions at $\sqrt{s_{NN}} = 5.02$ TeV”, *JHEP* **12** (2022) 126, arXiv:2202.00815 [nucl-ex].
- [22] CMS Collaboration, A. M. Sirunyan *et al.*, “Nuclear modification factor of D^0 mesons in PbPb collisions at $\sqrt{s_{NN}} = 5.02$ TeV”, *Phys. Lett. B* **782** (2018) 474–496, arXiv:1708.04962 [nucl-ex].
- [23] CMS Collaboration, A. M. Sirunyan *et al.*, “Measurement of the B^\pm Meson Nuclear Modification Factor in Pb–Pb Collisions at $\sqrt{s_{NN}} = 5.02$ TeV”, *Phys. Rev. Lett.* **119** (2017) 152301, arXiv:1705.04727 [hep-ex].
- [24] CMS Collaboration, A. M. Sirunyan *et al.*, “Measurement of prompt and nonprompt charmonium suppression in PbPb collisions at 5.02 TeV”, *Eur. Phys. J. C* **78** (2018) 509, arXiv:1712.08959 [nucl-ex].
- [25] CMS Collaboration, A. M. Sirunyan *et al.*, “Studies of Beauty Suppression via Nonprompt D^0 Mesons in Pb–Pb Collisions at $\sqrt{s_{NN}} = 5.02$ TeV”, *Phys. Rev. Lett.* **123** (2019) 022001, arXiv:1810.11102 [hep-ex].

- [26] **CMS** Collaboration, A. M. Sirunyan *et al.*, “Measurement of B_s^0 meson production in pp and PbPb collisions at $\sqrt{s_{NN}} = 5.02$ TeV”, *Phys. Lett. B* **796** (2019) 168–190, arXiv:1810.03022 [hep-ex].
- [27] **CMS** Collaboration, A. M. Sirunyan *et al.*, “Production of Λ_c^+ baryons in proton-proton and lead-lead collisions at $\sqrt{s_{NN}} = 5.02$ TeV”, *Phys. Lett. B* **803** (2020) 135328, arXiv:1906.03322 [hep-ex].
- [28] **ALICE** Collaboration, J. Adam *et al.*, “Measurement of electrons from beauty-hadron decays in p-Pb collisions at $\sqrt{s_{NN}} = 5.02$ TeV and Pb-Pb collisions at $\sqrt{s_{NN}} = 2.76$ TeV”, *JHEP* **07** (2017) 052, arXiv:1609.03898 [nucl-ex].
- [29] **ATLAS** Collaboration, M. Aaboud *et al.*, “Prompt and non-prompt J/ψ and $\psi(2S)$ suppression at high transverse momentum in 5.02 TeV Pb+Pb collisions with the ATLAS experiment”, *Eur. Phys. J. C* **78** (2018) 762, arXiv:1805.04077 [nucl-ex].
- [30] **ATLAS** Collaboration, G. Aad *et al.*, “Measurement of the nuclear modification factor for muons from charm and bottom hadrons in Pb+Pb collisions at 5.02 TeV with the ATLAS detector”, *Phys. Lett. B* **829** (2022) 137077, arXiv:2109.00411 [nucl-ex].
- [31] **STAR** Collaboration, J. Adam *et al.*, “Centrality and transverse momentum dependence of D^0 -meson production at mid-rapidity in Au+Au collisions at $\sqrt{s_{NN}} = 200$ GeV”, *Phys. Rev. C* **99** (2019) 034908, arXiv:1812.10224 [nucl-ex].
- [32] **STAR** Collaboration, S. Collaboration *et al.*, “Evidence of Mass Ordering of Charm and Bottom Quark Energy Loss in Au+Au Collisions at RHIC”, *Eur. Phys. J. C* **82** (2022) 1150, arXiv:2111.14615 [nucl-ex]. [Erratum: Eur.Phys.J.C 83, 455 (2023)].
- [33] **PHENIX** Collaboration, A. Adare *et al.*, “Single electron yields from semileptonic charm and bottom hadron decays in Au+Au collisions at $\sqrt{s_{NN}} = 200$ GeV”, *Phys. Rev. C* **93** (2016) 034904, arXiv:1509.04662 [nucl-ex].
- [34] Y. L. Dokshitzer, V. A. Khoze, and S. I. Troian, “On specific QCD properties of heavy quark fragmentation (‘dead cone’)”, *J. Phys. G* **17** (1991) 1602–1604.
- [35] **ALICE** Collaboration, S. Acharya *et al.*, “Direct observation of the dead-cone effect in QCD”, *Nature* **605** (2022) 440–446, arXiv:2106.05713 [nucl-ex]. [Erratum: Nature 607, E22 (2022)].
- [36] B. Svetitsky, “Diffusion of charmed quarks in the quark-gluon plasma”, *Phys. Rev. D* **37** (1988) 2484–2491.
- [37] **ALICE** Collaboration, S. Acharya *et al.*, “Transverse-momentum and event-shape dependence of D-meson flow harmonics in Pb–Pb collisions at $\sqrt{s_{NN}} = 5.02$ TeV”, *Phys. Lett. B* **813** (2021) 136054, arXiv:2005.11131 [nucl-ex].
- [38] A. Beraudo *et al.*, “Extraction of Heavy-Flavor Transport Coefficients in QCD Matter”, *Nucl. Phys. A* **979** (2018) 21–86, arXiv:1803.03824 [nucl-th].
- [39] J. Rafelski and B. Muller, “Strangeness Production in the Quark - Gluon Plasma”, *Phys. Rev. Lett.* **48** (1982) 1066. [Erratum: Phys. Rev. Lett. 56, 2334 (1986)].
- [40] P. Koch, B. Muller, and J. Rafelski, “Strangeness in Relativistic Heavy Ion Collisions”, *Phys. Rept.* **142** (1986) 167–262.

- [41] **STAR** Collaboration, J. Adam *et al.*, “Observation of D_s^\pm/D^0 enhancement in Au+Au collisions at $\sqrt{s_{NN}} = 200$ GeV”, *Phys. Rev. Lett.* **127** (2021) 092301, arXiv:2101.11793 [hep-ex].
- [42] **ALICE** Collaboration, S. Acharya *et al.*, “Measurement of D^0 , D^+ , D^{*+} and D_s^+ production in Pb–Pb collisions at $\sqrt{s_{NN}} = 5.02$ TeV”, *JHEP* **10** (2018) 174, arXiv:1804.09083 [nucl-ex].
- [43] **CMS** Collaboration, A. Tumasyan *et al.*, “Observation of B_s^0 mesons and measurement of the B_s^0/B^+ yield ratio in PbPb collisions at Image 1 TeV”, *Phys. Lett. B* **829** (2022) 137062, arXiv:2109.01908 [hep-ex].
- [44] **STAR** Collaboration, J. Adam *et al.*, “First measurement of Λ_c baryon production in Au+Au collisions at $\sqrt{s_{NN}} = 200$ GeV”, *Phys. Rev. Lett.* **124** (2020) 172301, arXiv:1910.14628 [nucl-ex].
- [45] **ALICE** Collaboration, J. Adam *et al.*, “ J/ψ suppression at forward rapidity in Pb–Pb collisions at $\sqrt{s_{NN}} = 5.02$ TeV”, *Phys. Lett. B* **766** (2017) 212–224, arXiv:1606.08197 [nucl-ex].
- [46] **ALICE** Collaboration, S. Acharya *et al.*, “Studies of J/ψ production at forward rapidity in Pb–Pb collisions at $\sqrt{s_{NN}} = 5.02$ TeV”, *JHEP* **02** (2020) 041, arXiv:1909.03158 [nucl-ex].
- [47] **ALICE** Collaboration, S. Acharya *et al.*, “Centrality and transverse momentum dependence of inclusive J/ψ production at midrapidity in Pb–Pb collisions at $\sqrt{s_{NN}} = 5.02$ TeV”, *Phys. Lett. B* **805** (2020) 135434, arXiv:1910.14404 [nucl-ex].
- [48] **ALICE** Collaboration, S. Acharya *et al.*, “Observation of a multiplicity dependence in the p_T -differential charm baryon-to-meson ratios in proton-proton collisions at $\sqrt{s} = 13$ TeV”, *Phys. Lett. B* **829** (2022) 137065, arXiv:2111.11948 [nucl-ex].
- [49] **LHCb** Collaboration, “Evidence for modification of b quark hadronization in high-multiplicity pp collisions at $\sqrt{s} = 13$ TeV”, arXiv:2204.13042 [hep-ex].
- [50] **ALICE** Collaboration, J. Adam *et al.*, “Enhanced production of multi-strange hadrons in high-multiplicity proton-proton collisions”, *Nature Phys.* **13** (2017) 535–539, arXiv:1606.07424 [nucl-ex].
- [51] **Particle Data Group** Collaboration, P. Zyla *et al.*, “Review of Particle Physics”, *PTEP* **2020** (2020) 083C01.
- [52] **ALICE** Collaboration, S. Acharya *et al.*, “Measurement of beauty and charm production in pp collisions at $\sqrt{s} = 5.02$ TeV via non-prompt and prompt D mesons”, *JHEP* **05** (2021) 220, arXiv:2102.13601 [nucl-ex].
- [53] **ALICE** Collaboration, K. Aamodt *et al.*, “Alignment of the ALICE Inner Tracking System with cosmic-ray tracks”, *JINST* **5** (2010) P03003, arXiv:1001.0502 [physics.ins-det].
- [54] J. Alme *et al.*, “The ALICE TPC, a large 3-dimensional tracking device with fast readout for ultra-high multiplicity events”, *Nucl. Instrum. Meth. A* **622** (2010) 316–367, arXiv:1001.1950 [physics.ins-det].
- [55] A. Akindinov *et al.*, “Performance of the ALICE Time-Of-Flight detector at the LHC”, *Eur. Phys. J. Plus* **128** (2013) 44.
- [56] **ALICE** Collaboration, E. Abbas *et al.*, “Performance of the ALICE VZERO system”, *JINST* **8** (2013) P10016, arXiv:1306.3130 [nucl-ex].

- [57] ALICE Collaboration, B. Abelev *et al.*, “Performance of the ALICE Experiment at the CERN LHC”, *Int. J. Mod. Phys. A* **29** (2014) 1430044, arXiv:1402.4476 [nucl-ex].
- [58] ALICE Collaboration, J. Adam *et al.*, “Centrality dependence of the charged-particle multiplicity density at midrapidity in Pb-Pb collisions at $\sqrt{s_{NN}} = 5.02$ TeV”, *Phys. Rev. Lett.* **116** (2016) 222302, arXiv:1512.06104 [nucl-ex].
- [59] C. Loizides, J. Kamin, and D. d’Enterria, “Improved Monte Carlo Glauber predictions at present and future nuclear colliders”, *Phys. Rev. C* **97** (2018) 054910, arXiv:1710.07098 [nucl-ex]. [Erratum: *Phys.Rev.C* 99, 019901 (2019)].
- [60] D. d’Enterria and C. Loizides, “Progress in the Glauber Model at Collider Energies”, *Ann. Rev. Nucl. Part. Sci.* **71** (2021) 315–344, arXiv:2011.14909 [hep-ph].
- [61] T. Chen and C. Guestrin, “Xgboost: A scalable tree boosting system”, in *Proceedings of the 22nd ACM SIGKDD International Conference on Knowledge Discovery and Data Mining, KDD ’16*, p. 785–794. New York, NY, USA, 2016. arXiv:1603.02754 [cs.LG].
- [62] L. Barioglio, F. Catalano, M. Concas, P. Fecchio, F. Grosa, F. Mazzaschi, and M. Puccio, “hipe4ml/hipe4ml”, July, 2021. <https://doi.org/10.5281/zenodo.5070132>.
- [63] X.-N. Wang and M. Gyulassy, “Hijing: A monte carlo model for multiple jet production in pp, pA, and AA collisions”, *Phys. Rev. D* **44** (Dec, 1991) 3501–3516.
- [64] T. Sjostrand, S. Mrenna, and P. Z. Skands, “PYTHIA 6.4 Physics and Manual”, *JHEP* **05** (2006) 026, arXiv:hep-ph/0603175.
- [65] T. Sjöstrand, S. Ask, J. R. Christiansen, R. Corke, N. Desai, P. Ilten, S. Mrenna, S. Prestel, C. O. Rasmussen, and P. Z. Skands, “An introduction to PYTHIA 8.2”, *Comput. Phys. Commun.* **191** (2015) 159–177, arXiv:1410.3012 [hep-ph].
- [66] P. Skands, S. Carrazza, and J. Rojo, “Tuning PYTHIA 8.1: the Monash 2013 Tune”, *Eur. Phys. J. C* **74** (2014) 3024, arXiv:1404.5630 [hep-ph].
- [67] R. Brun, F. Bruyant, F. Carminati, S. Giani, M. Maire, A. McPherson, G. Patrick, and L. Urban, *GEANT: Detector Description and Simulation Tool; Oct 1994*. CERN Program Library. CERN, Geneva, 1993. <http://cds.cern.ch/record/1082634>. Long Writeup W5013.
- [68] M. Cacciari, M. Greco, and P. Nason, “The p_T spectrum in heavy-flavor hadroproduction”, *JHEP* **05** (1998) 007, arXiv:hep-ph/9803400 [hep-ph].
- [69] M. Cacciari, S. Frixione, and P. Nason, “The p_T spectrum in heavy-flavor photoproduction”, *JHEP* **03** (2001) 006, arXiv:hep-ph/0102134 [hep-ph].
- [70] M. He, R. J. Fries, and R. Rapp, “Heavy Flavor at the Large Hadron Collider in a Strong Coupling Approach”, *Phys. Lett. B* **735** (2014) 445–450, arXiv:1401.3817 [nucl-th].
- [71] M. He and R. Rapp, “Hadronization and Charm-Hadron Ratios in Heavy-Ion Collisions”, *Phys. Rev. Lett.* **124** (2020) 042301, arXiv:1905.09216 [nucl-th].
- [72] ALICE Collaboration, J. Adam *et al.*, “Transverse momentum dependence of D-meson production in Pb-Pb collisions at $\sqrt{s_{NN}} = 2.76$ TeV”, *JHEP* **03** (2016) 081, arXiv:1509.06888 [nucl-ex].
- [73] ALICE Collaboration, “ALICE 2017 luminosity determination for pp collisions at $\sqrt{s} = 5$ TeV”, *ALICE-PUBLIC-2018-014* (Nov, 2018) . <http://cds.cern.ch/record/2648933>.





- [74] W. Ke, Y. Xu, and S. A. Bass, “Linearized Boltzmann-Langevin model for heavy quark transport in hot and dense QCD matter”, *Phys. Rev. C* **98** (2018) 064901, arXiv:1806.08848 [nucl-th].

A The ALICE Collaboration

S. Acharya ^{123,131}, D. Adamová ⁸⁵, A. Adler⁶⁹, G. Aglieri Rinella ³², M. Agnello ²⁹, N. Agrawal ⁵⁰, Z. Ahammed ¹³¹, S. Ahmad ¹⁵, S.U. Ahn ⁷⁰, I. Ahuja ³⁷, A. Akindinov ¹³⁹, M. Al-Turany ⁹⁷, D. Aleksandrov ¹³⁹, B. Alessandro ⁵⁵, H.M. Alfanda ⁶, R. Alfaro Molina ⁶⁶, B. Ali ¹⁵, Y. Ali¹³, A. Alici ²⁵, N. Alizadehvandchali ¹¹², A. Alkin ³², J. Alme ²⁰, G. Alocco ⁵¹, T. Alt ⁶³, I. Altsybeev ¹³⁹, M.N. Anaam ⁶, C. Andrei ⁴⁵, A. Andronic ¹³⁴, V. Anguelov ⁹⁴, F. Antinori ⁵³, P. Antonioli ⁵⁰, C. Anuj ¹⁵, N. Apadula ⁷³, L. Aphecetche ¹⁰², H. Appelshäuser ⁶³, S. Arcelli ²⁵, R. Arnaldi ⁵⁵, I.C. Arsene ¹⁹, M. Arslanok ¹³⁶, A. Augustinus ³², R. Averbeck ⁹⁷, S. Aziz ¹²⁷, M.D. Azmi ¹⁵, A. Badalà ⁵², Y.W. Baek ⁴⁰, X. Bai ⁹⁷, R. Bailhache ⁶³, Y. Bailung ⁴⁷, R. Bala ⁹⁰, A. Balbino ²⁹, A. Baldisseri ¹²⁶, B. Balis ², D. Banerjee ⁴, Z. Banoo ⁹⁰, R. Barbera ²⁶, L. Barioglio ⁹⁵, M. Barlou⁷⁷, G.G. Barnaföldi ¹³⁵, L.S. Barnby ⁸⁴, V. Barret ¹²³, L. Barreto ¹⁰⁸, C. Bartels ¹¹⁵, K. Barth ³², E. Bartsch ⁶³, F. Baruffaldi ²⁷, N. Bastid ¹²³, S. Basu ⁷⁴, G. Batigne ¹⁰², D. Battistini ⁹⁵, B. Batyunya ¹⁴⁰, D. Bauri⁴⁶, J.L. Bazo Alba ¹⁰⁰, I.G. Bearden ⁸², C. Beattie ¹³⁶, P. Becht ⁹⁷, D. Behera ⁴⁷, I. Belikov ¹²⁵, A.D.C. Bell Hechavarria ¹³⁴, F. Bellini ²⁵, R. Bellwied ¹¹², S. Belokurova ¹³⁹, V. Belyaev ¹³⁹, G. Bencedi ^{135,64}, S. Beole ²⁴, A. Bercuci ⁴⁵, Y. Berdnikov ¹³⁹, A. Berdnikova ⁹⁴, L. Bergmann ⁹⁴, M.G. Besoiu ⁶², L. Betev ³², P.P. Bhaduri ¹³¹, A. Bhasin ⁹⁰, I.R. Bhat⁹⁰, M.A. Bhat ⁴, B. Bhattacharjee ⁴¹, L. Bianchi ²⁴, N. Bianchi ⁴⁸, J. Bielčik ³⁵, J. Bielčíková ⁸⁵, J. Biernat ¹⁰⁵, A. Bilandzic ⁹⁵, G. Biro ¹³⁵, S. Biswas ⁴, J.T. Blair ¹⁰⁶, D. Blau ¹³⁹, M.B. Blidaru ⁹⁷, N. Bluhme³⁸, C. Blume ⁶³, G. Boca ^{21,54}, F. Bock ⁸⁶, T. Bodova ²⁰, A. Bogdanov¹³⁹, S. Boi ²², J. Bok ⁵⁷, L. Boldizsár ¹³⁵, A. Bolozdynya ¹³⁹, M. Bombara ³⁷, P.M. Bond ³², G. Bonomi ^{130,54}, H. Borel ¹²⁶, A. Borissov ¹³⁹, H. Bossi ¹³⁶, E. Botta ²⁴, L. Bratrud ⁶³, P. Braun-Munzinger ⁹⁷, M. Bregant ¹⁰⁸, M. Broz ³⁵, G.E. Bruno ^{96,31}, M.D. Buckland ¹¹⁵, D. Budnikov ¹³⁹, H. Buesching ⁶³, S. Bufalino ²⁹, O. Bugnon¹⁰², P. Buhler ¹⁰¹, Z. Buthelezi ^{67,119}, J.B. Butt¹³, A. Bylinkin ¹¹⁴, S.A. Bysiak¹⁰⁵, M. Cai ^{27,6}, H. Caines ¹³⁶, A. Caliva ⁹⁷, E. Calvo Villar ¹⁰⁰, J.M.M. Camacho ¹⁰⁷, P. Camerini ²³, F.D.M. Canedo ¹⁰⁸, M. Carabas ¹²², F. Carnesecchi ³², R. Caron ^{124,126}, J. Castillo Castellanos ¹²⁶, F. Catalano ²⁹, C. Ceballos Sanchez ¹⁴⁰, I. Chakaberia ⁷³, P. Chakraborty ⁴⁶, S. Chandra ¹³¹, S. Chapeland ³², M. Chartier ¹¹⁵, S. Chattopadhyay ¹³¹, S. Chattopadhyay ⁹⁸, T.G. Chavez ⁴⁴, T. Cheng ⁶, C. Cheshkov ¹²⁴, B. Cheynis ¹²⁴, V. Chibante Barroso ³², D.D. Chinellato ¹⁰⁹, E.S. Chizzali ^{11,95}, J. Cho ⁵⁷, S. Cho ⁵⁷, P. Chochula ³², P. Christakoglou ⁸³, C.H. Christensen ⁸², P. Christiansen ⁷⁴, T. Chujo ¹²¹, M. Ciacco ²⁹, C. Cicalo ⁵¹, L. Cifarelli ²⁵, F. Cindolo ⁵⁰, M.R. Ciupek⁹⁷, G. Clai^{III,50}, F. Colamaria ⁴⁹, J.S. Colburn⁹⁹, D. Colella ^{96,31}, A. Collu⁷³, M. Colocci ³², M. Concas ^{IV,55}, G. Conesa Balbastre ⁷², Z. Conesa del Valle ¹²⁷, G. Contin ²³, J.G. Contreras ³⁵, M.L. Coquet ¹²⁶, T.M. Cormier^{I,86}, P. Cortese ^{129,55}, M.R. Cosentino ¹¹⁰, F. Costa ³², S. Costanza ^{21,54}, P. Crochet ¹²³, R. Cruz-Torres ⁷³, E. Cuautle⁶⁴, P. Cui ⁶, L. Cunqueiro⁸⁶, A. Dainese ⁵³, M.C. Danisch ⁹⁴, A. Danu ⁶², P. Das ⁷⁹, P. Das ⁴, S. Das ⁴, S. Dash ⁴⁶, R.M.H. David⁴⁴, A. De Caro ²⁸, G. de Cataldo ⁴⁹, L. De Cilladi ²⁴, J. de Cuveland³⁸, A. De Falco ²², D. De Gruttola ²⁸, N. De Marco ⁵⁵, C. De Martin ²³, S. De Pasquale ²⁸, S. Deb ⁴⁷, H.F. Degenhardt¹⁰⁸, K.R. Deja¹³², R. Del Grande ⁹⁵, L. Dello Stritto ²⁸, W. Deng ⁶, P. Dhankher ¹⁸, D. Di Bari ³¹, A. Di Mauro ³², R.A. Diaz ^{140,7}, T. Dietel ¹¹¹, Y. Ding ^{124,6}, R. Divià ³², D.U. Dixit ¹⁸, Ø. Djuvsland²⁰, U. Dmitrieva ¹³⁹, A. Dobrin ⁶², B. Dönigus ⁶³, A.K. Dubey ¹³¹, J.M. Dubinski ¹³², A. Dubla ⁹⁷, S. Dudi ⁸⁹, P. Dupieux ¹²³, M. Durkac¹⁰⁴, N. Dzalaiova¹², T.M. Eder ¹³⁴, R.J. Ehlers ⁸⁶, V.N. Eikeland²⁰, F. Eisenhut ⁶³, D. Elia ⁴⁹, B. Erasmus ¹⁰², F. Ercolessi ²⁵, F. Erhardt ⁸⁸, M.R. Ersdal²⁰, B. Espagnon ¹²⁷, G. Eulisse ³², D. Evans ⁹⁹, S. Evdokimov ¹³⁹, L. Fabbietti ⁹⁵, M. Faggin ²⁷, J. Faivre ⁷², F. Fan ⁶, W. Fan ⁷³, A. Fantoni ⁴⁸, M. Fasel ⁸⁶, P. Fedchio²⁹, A. Feliciello ⁵⁵, G. Feofilov ¹³⁹, A. Fernández Téllez ⁴⁴, M.B. Ferrer ³², A. Ferrero ¹²⁶, A. Ferretti ²⁴, V.J.G. Feuillard ⁹⁴, J. Figiel ¹⁰⁵, V. Filova ³⁵, D. Finogeev ¹³⁹, F.M. Fionda ⁵¹, G. Fiorenza⁹⁶, F. Flor ¹¹², A.N. Flores ¹⁰⁶, S. Foertsch ⁶⁷, I. Fokin ⁹⁴, S. Fokin ¹³⁹, E. Fragiaco ⁵⁶, E. Frajna ¹³⁵, U. Fuchs ³², N. Funicello ²⁸, C. Furget ⁷², A. Furs ¹³⁹, J.J. Gaardhøje ⁸², M. Gagliardi ²⁴, A.M. Gago ¹⁰⁰, A. Gal¹²⁵, C.D. Galvan ¹⁰⁷, P. Ganoti ⁷⁷, C. Garabatos ⁹⁷, J.R.A. Garcia ⁴⁴, E. Garcia-Solis ⁹, K. Garg ¹⁰², C. Gargiulo ³², A. Garibli⁸⁰, K. Garner¹³⁴, E.F. Gauger ¹⁰⁶, A. Gautam ¹¹⁴, M.B. Gay Ducati ⁶⁵, M. Germain ¹⁰², S.K. Ghosh⁴, M. Giacalone ²⁵, P. Gianotti ⁴⁸, P. Giubellino ^{97,55}, P. Giubilato ²⁷, A.M.C. Glaenger ¹²⁶, P. Glässel ⁹⁴, E. Glimos ¹¹⁸, D.J.Q. Goh⁷⁵, V. Gonzalez ¹³³, L.H. González-Trueba ⁶⁶, S. Gorbunov³⁸, M. Gorgon ², L. Görlich ¹⁰⁵, S. Gotovac³³, V. Grabski ⁶⁶, L.K. Graczykowski ¹³², E. Grecka ⁸⁵, L. Greiner ⁷³, A. Grelli ⁵⁸, C. Grigoras ³², V. Grigoriev ¹³⁹, S. Grigoryan ^{140,1}, F. Grosa ³², J.F. Grosse-Oetringhaus ³², R. Grosso ⁹⁷, D. Grund ³⁵, G.G. Guardiano ¹⁰⁹, R. Guernane ⁷², M. Guilbaud ¹⁰², K. Gulbrandsen ⁸², T. Gunji ¹²⁰, W. Guo ⁶,

A. Gupta ⁹⁰, R. Gupta ⁹⁰, S.P. Guzman ⁴⁴, L. Gyulai ¹³⁵, M.K. Habib ⁹⁷, C. Hadjidakis ¹²⁷, H. Hamagaki ⁷⁵, M. Hamid ⁶, Y. Han ¹³⁷, R. Hannigan ¹⁰⁶, M.R. Haque ¹³², A. Harlenderova ⁹⁷, J.W. Harris ¹³⁶, A. Harton ⁹, J.A. Hasenbichler ³², H. Hassan ⁸⁶, D. Hatzifotiadou ⁵⁰, P. Hauer ⁴², L.B. Havener ¹³⁶, S.T. Heckel ⁹⁵, E. Hellbär ⁹⁷, H. Helstrup ³⁴, T. Herman ³⁵, G. Herrera Corral ⁸, F. Herrmann ¹³⁴, K.F. Hetland ³⁴, B. Heybeck ⁶³, H. Hillemanns ³², C. Hills ¹¹⁵, B. Hippolyte ¹²⁵, B. Hofman ⁵⁸, B. Hohlweger ⁸³, J. Honermann ¹³⁴, G.H. Hong ¹³⁷, D. Horak ³⁵, A. Horzyk ², R. Hosokawa ¹⁴, Y. Hou ⁶, P. Hristov ³², C. Hughes ¹¹⁸, P. Huhn ⁶³, L.M. Huhta ¹¹³, C.V. Hulse ¹²⁷, T.J. Humanic ⁸⁷, H. Hushnud ⁹⁸, A. Hutson ¹¹², D. Hutter ³⁸, J.P. Iddon ¹¹⁵, R. Ilkaev ¹³⁹, H. Ilyas ¹³, M. Inaba ¹²¹, G.M. Innocenti ³², M. Ippolitov ¹³⁹, A. Isakov ⁸⁵, T. Isidori ¹¹⁴, M.S. Islam ⁹⁸, M. Ivanov ⁹⁷, V. Ivanov ¹³⁹, V. Izucheev ¹³⁹, M. Jablonski ², B. Jacak ⁷³, N. Jacazio ³², P.M. Jacobs ⁷³, S. Jadlovská ¹⁰⁴, J. Jadlovsky ¹⁰⁴, L. Jaffe ³⁸, C. Jahnke ¹⁰⁹, M.A. Janik ¹³², T. Janson ⁶⁹, M. Jercic ⁸⁸, O. Jevons ⁹⁹, A.A.P. Jimenez ⁶⁴, F. Jonas ⁸⁶, P.G. Jones ⁹⁹, J.M. Jowett ^{32,97}, J. Jung ⁶³, M. Jung ⁶³, A. Junique ³², A. Jusko ⁹⁹, M.J. Kabus ^{32,132}, J. Kaewjai ¹⁰³, P. Kalinak ⁵⁹, A.S. Kalteyer ⁹⁷, A. Kalweit ³², V. Kaplin ¹³⁹, A. Karasu Uysal ⁷¹, D. Karatovic ⁸⁸, O. Karavichev ¹³⁹, T. Karavicheva ¹³⁹, P. Karczmarczyk ¹³², E. Karpechev ¹³⁹, V. Kashyap ⁷⁹, A. Kazantsev ¹³⁹, U. Keschull ⁶⁹, R. Keidel ¹³⁸, D.L.D. Keijdener ⁵⁸, M. Keil ³², B. Ketzer ⁴², A.M. Khan ⁶, S. Khan ¹⁵, A. Khanzadeev ¹³⁹, Y. Kharlov ¹³⁹, A. Khatun ¹⁵, A. Khuntia ¹⁰⁵, B. Kileng ³⁴, B. Kim ¹⁶, C. Kim ¹⁶, D.J. Kim ¹¹³, E.J. Kim ⁶⁸, J. Kim ¹³⁷, J.S. Kim ⁴⁰, J. Kim ⁹⁴, J. Kim ⁶⁸, M. Kim ⁹⁴, S. Kim ¹⁷, T. Kim ¹³⁷, S. Kirsch ⁶³, I. Kisel ³⁸, S. Kiselev ¹³⁹, A. Kisiel ¹³², J.P. Kitowski ², J.L. Klay ⁵, J. Klein ³², S. Klein ⁷³, C. Klein-Bösing ¹³⁴, M. Kleiner ⁶³, T. Klemenz ⁹⁵, A. Kluge ³², A.G. Knospe ¹¹², C. Kobdaj ¹⁰³, T. Kollegger ⁹⁷, A. Kondratyev ¹⁴⁰, N. Kondratyeva ¹³⁹, E. Kondratyuk ¹³⁹, J. Konig ⁶³, S.A. Konigstorfer ⁹⁵, P.J. Konopka ³², G. Kornakov ¹³², S.D. Koryciak ², A. Kotliarov ⁸⁵, O. Kovalenko ⁷⁸, V. Kovalenko ¹³⁹, M. Kowalski ¹⁰⁵, I. Králík ⁵⁹, A. Kravčáková ³⁷, L. Kreis ⁹⁷, M. Krivda ^{99,59}, F. Krizek ⁸⁵, K. Krizkova Gajdosova ³⁵, M. Kroesen ⁹⁴, M. Krüger ⁶³, D.M. Krupova ³⁵, E. Kryshen ¹³⁹, M. Krzewicki ³⁸, V. Kučera ³², C. Kuhn ¹²⁵, P.G. Kuijter ⁸³, T. Kumaoka ¹²¹, D. Kumar ¹³¹, L. Kumar ⁸⁹, N. Kumar ⁸⁹, S. Kundu ³², P. Kurashvili ⁷⁸, A. Kurepin ¹³⁹, A.B. Kurepin ¹³⁹, S. Kushpil ⁸⁵, J. Kvapil ⁹⁹, M.J. Kweon ⁵⁷, J.Y. Kwon ⁵⁷, Y. Kwon ¹³⁷, S.L. La Pointe ³⁸, P. La Rocca ²⁶, Y.S. Lai ⁷³, A. Lakrathok ¹⁰³, M. Lamanna ³², R. Langoy ¹¹⁷, P. Larionov ⁴⁸, E. Laudi ³², L. Lautner ^{32,95}, R. Lavicka ¹⁰¹, T. Lazareva ¹³⁹, R. Lea ^{130,54}, J. Lehrbach ³⁸, R.C. Lemmon ⁸⁴, I. León Monzón ¹⁰⁷, M.M. Lesch ⁹⁵, E.D. Lesser ¹⁸, M. Lettrich ⁹⁵, P. Lévai ¹³⁵, X. Li ¹⁰, X.L. Li ⁶, J. Lien ¹¹⁷, R. Lietava ⁹⁹, B. Lim ¹⁶, S.H. Lim ¹⁶, V. Lindenstruth ³⁸, A. Lindner ⁴⁵, C. Lippmann ⁹⁷, A. Liu ¹⁸, D.H. Liu ⁶, J. Liu ¹¹⁵, I.M. Lofnes ²⁰, V. Loginov ¹³⁹, C. Loizides ⁸⁶, P. Loncar ³³, J.A. Lopez ⁹⁴, X. Lopez ¹²³, E. López Torres ⁷, P. Lu ^{97,116}, J.R. Luhder ¹³⁴, M. Lunardon ²⁷, G. Luparello ⁵⁶, Y.G. Ma ³⁹, A. Maevskaya ¹³⁹, M. Mager ³², T. Mahmoud ⁴², A. Maire ¹²⁵, M. Malaev ¹³⁹, N.M. Malik ⁹⁰, Q.W. Malik ¹⁹, S.K. Malik ⁹⁰, L. Malinina ^{I,VII,140}, D. Mal'Kevich ¹³⁹, D. Mallick ⁷⁹, N. Mallick ⁴⁷, G. Mandaglio ^{30,52}, V. Manko ¹³⁹, F. Manso ¹²³, V. Manzari ⁴⁹, Y. Mao ⁶, G.V. Margagliotti ²³, A. Margotti ⁵⁰, A. Marín ⁹⁷, C. Markert ¹⁰⁶, M. Marquard ⁶³, N.A. Martin ⁹⁴, P. Martinengo ³², J.L. Martinez ¹¹², M.I. Martínez ⁴⁴, G. Martínez García ¹⁰², S. Masciocchi ⁹⁷, M. Masea ²⁴, A. Masoni ⁵¹, L. Massacrier ¹²⁷, A. Mastroserio ^{128,49}, A.M. Mathis ⁹⁵, O. Matonoha ⁷⁴, P.F.T. Matuoka ¹⁰⁸, A. Matyja ¹⁰⁵, C. Mayer ¹⁰⁵, A.L. Mazuecos ³², F. Mazzaschi ²⁴, M. Mazzilli ³², J.E. Mdhuli ¹¹⁹, A.F. Mechler ⁶³, Y. Melikyan ¹³⁹, A. Menchaca-Rocha ⁶⁶, E. Meninno ^{101,28}, A.S. Menon ¹¹², M. Meres ¹², S. Mhlanga ^{111,67}, Y. Miake ¹²¹, L. Micheletti ⁵⁵, L.C. Migliorin ¹²⁴, D.L. Mihaylov ⁹⁵, K. Mikhaylov ^{140,139}, A.N. Mishra ¹³⁵, D. Miśkowiec ⁹⁷, A. Modak ⁴, A.P. Mohanty ⁵⁸, B. Mohanty ⁷⁹, M. Mohisin Khan ^{V,15}, M.A. Molander ⁴³, Z. Moravcova ⁸², C. Mordasini ⁹⁵, D.A. Moreira De Godoy ¹³⁴, I. Morozov ¹³⁹, A. Morsch ³², T. Mrnjavac ³², V. Muccifora ⁴⁸, E. Mudnic ³³, S. Muhuri ¹³¹, J.D. Mulligan ⁷³, A. Mulliri ²², M.G. Munhoz ¹⁰⁸, R.H. Munzer ⁶³, H. Murakami ¹²⁰, S. Murray ¹¹¹, L. Musa ³², J. Musinsky ⁵⁹, J.W. Myrcha ¹³², B. Naik ¹¹⁹, R. Nair ⁷⁸, B.K. Nandi ⁴⁶, R. Nania ⁵⁰, E. Nappi ⁴⁹, A.F. Nassirpour ⁷⁴, A. Nath ⁹⁴, C. Nattrass ¹¹⁸, A. Neagu ¹⁹, A. Negru ¹²², L. Nellen ⁶⁴, S.V. Nesbo ³⁴, G. Neskovic ³⁸, D. Nesterov ¹³⁹, B.S. Nielsen ⁸², E.G. Nielsen ⁸², S. Nikolaev ¹³⁹, S. Nikulin ¹³⁹, V. Nikulin ¹³⁹, F. Noferini ⁵⁰, S. Noh ¹¹, P. Nomokonov ¹⁴⁰, J. Norman ¹¹⁵, N. Novitzky ¹²¹, P. Nowakowski ¹³², A. Nyanin ¹³⁹, J. Nystrand ²⁰, M. Ogino ⁷⁵, A. Ohlson ⁷⁴, V.A. Okorokov ¹³⁹, J. Oleniacz ¹³², A.C. Oliveira Da Silva ¹¹⁸, M.H. Oliver ¹³⁶, A. Onnerstad ¹¹³, C. Oppedisano ⁵⁵, A. Ortiz Velasquez ⁶⁴, A. Oskarsson ⁷⁴, J. Otwinowski ¹⁰⁵, M. Oya ⁹², K. Oyama ⁷⁵, Y. Pachmayer ⁹⁴, S. Padhan ⁴⁶, D. Pagano ^{130,54}, G. Paić ⁶⁴, A. Palasciano ⁴⁹, S. Panebianco ¹²⁶, J. Park ⁵⁷, J.E. Parkkila ^{32,113}, S.P. Pathak ¹¹², R.N. Patra ⁹⁰, B. Paul ²², H. Pei ⁶, T. Peitzmann ⁵⁸,

X. Peng⁶, L.G. Pereira⁶⁵, H. Pereira Da Costa¹²⁶, D. Peresunko¹³⁹, G.M. Perez⁷, S. Perrin¹²⁶, Y. Pestov¹³⁹, V. Petráček³⁵, V. Petrov¹³⁹, M. Petrovici⁴⁵, R.P. Pezzi^{102,65}, S. Piano⁵⁶, M. Pikna¹², P. Pillot¹⁰², O. Pinazza^{50,32}, L. Pinsky¹¹², C. Pinto^{95,26}, S. Pisano⁴⁸, M. Płoskoń⁷³, M. Planinic⁸⁸, F. Pliquet⁶³, M.G. Poghosyan⁸⁶, S. Politano²⁹, N. Poljak⁸⁸, A. Pop⁴⁵, S. Porteboeuf-Houssais¹²³, J. Porter⁷³, V. Pozdniakov¹⁴⁰, S.K. Prasad⁴, S. Prasad⁴⁷, R. Preghenella⁵⁰, F. Prino⁵⁵, C.A. Pruneau¹³³, I. Pshenichnov¹³⁹, M. Puccio³², S. Qiu⁸³, L. Quaglia²⁴, R.E. Quishpe¹¹², S. Ragoni⁹⁹, A. Rakotozafindrabe¹²⁶, L. Ramello^{129,55}, F. Rami¹²⁵, S.A.R. Ramirez⁴⁴, T.A. Rancien⁷², R. Raniwala⁹¹, S. Raniwala⁹¹, S.S. Räsänen⁴³, R. Rath⁴⁷, I. Ravasenga⁸³, K.F. Read^{86,118}, A.R. Redelbach³⁸, K. Redlich^{VI,78}, A. Rehman²⁰, P. Reichelt⁶³, F. Reidt³², H.A. Reme-Ness³⁴, Z. Rescakova³⁷, K. Reygers⁹⁴, A. Riabov¹³⁹, V. Riabov¹³⁹, R. Ricci²⁸, T. Richert⁷⁴, M. Richter¹⁹, W. Riegler³², F. Riggi²⁶, C. Ristea⁶², M. Rodríguez Cahuantzi⁴⁴, K. Røed¹⁹, R. Rogalev¹³⁹, E. Rogochaya¹⁴⁰, T.S. Rogoschinski⁶³, D. Rohr³², D. Röhrich²⁰, P.F. Rojas⁴⁴, S. Rojas Torres³⁵, P.S. Rokita¹³², F. Ronchetti⁴⁸, A. Rosano^{30,52}, E.D. Rosas⁶⁴, A. Rossi⁵³, A. Roy⁴⁷, P. Roy⁹⁸, S. Roy⁴⁶, N. Rubini²⁵, D. Ruggiano¹³², R. Rui²³, B. Rumyantsev¹⁴⁰, P.G. Russek², R. Russo⁸³, A. Rustamov⁸⁰, E. Ryabinkin¹³⁹, Y. Ryabov¹³⁹, A. Rybicki¹⁰⁵, H. Rytkonen¹¹³, W. Rzeska¹³², O.A.M. Saarimaki⁴³, R. Sadek¹⁰², S. Sadovsky¹³⁹, J. Saetre²⁰, K. Šafařík³⁵, S.K. Saha¹³¹, S. Saha⁷⁹, B. Sahoo⁴⁶, P. Sahoo⁴⁶, R. Sahoo⁴⁷, S. Sahoo⁶⁰, D. Sahu⁴⁷, P.K. Sahu⁶⁰, J. Saini¹³¹, K. Sajdakova³⁷, S. Sakai¹²¹, M.P. Salvan⁹⁷, S. Sambyal⁹⁰, T.B. Saramela¹⁰⁸, D. Sarkar¹³³, N. Sarkar¹³¹, P. Sarma⁴¹, V. Sarritzu²², V.M. Sarti⁹⁵, M.H.P. Sas¹³⁶, J. Schambach⁸⁶, H.S. Scheid⁶³, C. Schiaua⁴⁵, R. Schicker⁹⁴, A. Schmah⁹⁴, C. Schmidt⁹⁷, H.R. Schmidt⁹³, M.O. Schmidt³², M. Schmidt⁹³, N.V. Schmidt^{86,63}, A.R. Schmier¹¹⁸, R. Schotter¹²⁵, J. Schukraft³², K. Schwarz⁹⁷, K. Schweda⁹⁷, G. Scioli²⁵, E. Scomarini⁵⁵, J.E. Seger¹⁴, Y. Sekiguchi¹²⁰, D. Sekihata¹²⁰, I. Selyuzhenkov^{97,139}, S. Senyukov¹²⁵, J.J. Seo⁵⁷, D. Serebryakov¹³⁹, L. Šerkšnytė⁹⁵, A. Sevcenco⁶², T.J. Shaba⁶⁷, A. Shabanov¹³⁹, A. Shabetai¹⁰², R. Shahoyan³², W. Shaikh⁹⁸, A. Shangaraev¹³⁹, A. Sharma⁸⁹, D. Sharma⁴⁶, H. Sharma¹⁰⁵, M. Sharma⁹⁰, N. Sharma⁸⁹, S. Sharma⁹⁰, U. Sharma⁹⁰, A. Shatat¹²⁷, O. Sheibani¹¹², K. Shigaki⁹², M. Shimomura⁷⁶, S. Shirinkin¹³⁹, Q. Shou³⁹, Y. Sibiriak¹³⁹, S. Siddhanta⁵¹, T. Siemiarzuk⁷⁸, T.F. Silva¹⁰⁸, D. Silvermyr⁷⁴, T. Simantathammakul¹⁰³, R. Simeonov³⁶, G. Simonetti³², B. Singh⁹⁰, B. Singh⁹⁵, R. Singh⁷⁹, R. Singh⁹⁰, R. Singh⁴⁷, V.K. Singh¹³¹, V. Singhal¹³¹, T. Sinha⁹⁸, B. Sitar¹², M. Sitta^{129,55}, T.B. Skaali¹⁹, G. Skorodumovs⁹⁴, M. Slupecki⁴³, N. Smirnov¹³⁶, R.J.M. Snellings⁵⁸, E.H. Solheim¹⁹, C. Soncco¹⁰⁰, J. Song¹¹², A. Songmoolnak¹⁰³, F. Soramel²⁷, S.P. Sorensen¹¹⁸, R. Soto Camacho⁴⁴, R. Spijkers⁸³, I. Sputowska¹⁰⁵, J. Staa⁷⁴, J. Stachel⁹⁴, I. Stan⁶², P.J. Steffanic¹¹⁸, S.F. Stiefelmaier⁹⁴, D. Stocco¹⁰², I. Storehaug¹⁹, M.M. Stortvedt³⁴, P. Stratmann¹³⁴, S. Strazzi²⁵, C.P. Stylianidis⁸³, A.A.P. Suaide¹⁰⁸, C. Suire¹²⁷, M. Sukhanov¹³⁹, M. Suljic³², V. Sumberia⁹⁰, S. Sumowidagdo⁸¹, S. Swain⁶⁰, A. Szabo¹², I. Szarka¹², U. Tabassam¹³, S.F. Taghavi⁹⁵, G. Tallepied^{97,123}, J. Takahashi¹⁰⁹, G.J. Tambave²⁰, S. Tang^{123,6}, Z. Tang¹¹⁶, J.D. Tapia Takaki¹¹⁴, N. Tapus¹²², L.A. Tarasovicova¹³⁴, M.G. Tarzila⁴⁵, A. Tauro³², A. Telesca³², L. Terlizzi²⁴, C. Terrevoli¹¹², G. Tersimonov³, S. Thakur¹³¹, D. Thomas¹⁰⁶, R. Tieulent¹²⁴, A. Tikhonov¹³⁹, A.R. Timmins¹¹², M. Tkacik¹⁰⁴, T. Tkacik¹⁰⁴, A. Toia⁶³, N. Topilskaya¹³⁹, M. Toppi⁴⁸, F. Torales-Acosta¹⁸, T. Tork¹²⁷, A.G. Torres Ramos³¹, A. Trifiró^{30,52}, A.S. Triolo^{30,52}, S. Tripathy⁵⁰, T. Tripathy⁴⁶, S. Trogolo³², V. Trubnikov³, W.H. Trzaska¹¹³, T.P. Trzcinski¹³², R. Turrisi⁵³, T.S. Tveter¹⁹, K. Ullaland²⁰, B. Ulukutlu⁹⁵, A. Uras¹²⁴, M. Urioni^{54,130}, G.L. Usai²², M. Vala³⁷, N. Valle²¹, S. Vallero⁵⁵, L.V.R. van Doremalen⁵⁸, M. van Leeuwen⁸³, C.A. van Veen⁹⁴, R.J.G. van Weelden⁸³, P. Vande Vyvre³², D. Varga¹³⁵, Z. Varga¹³⁵, M. Varga-Kofarago¹³⁵, M. Vasileiou⁷⁷, A. Vasiliev¹³⁹, O. Vázquez Doce⁹⁵, O. Vazquez Rueda⁷⁴, V. Vechernin¹³⁹, E. Vercellin²⁴, S. Vergara Limón⁴⁴, L. Vermunt⁵⁸, R. Vértesi¹³⁵, M. Verweij⁵⁸, L. Vickovic³³, Z. Vilakazi¹¹⁹, O. Villalobos Baillie⁹⁹, G. Vino⁴⁹, A. Vinogradov¹³⁹, T. Virgili²⁸, V. Vislavicius⁸², A. Vodopyanov¹⁴⁰, B. Volkel³², M.A. Völkl⁹⁴, K. Voloshin¹³⁹, S.A. Voloshin¹³³, G. Volpe³¹, B. von Haller³², I. Vorobyev⁹⁵, N. Vozniuk¹³⁹, J. Vrláková³⁷, B. Wagner²⁰, C. Wang³⁹, D. Wang³⁹, M. Weber¹⁰¹, A. Wegrzynek³², F.T. Weiglhofer³⁸, S.C. Wenzel³², J.P. Wessels¹³⁴, S.L. Weyhiller¹³⁶, J. Wiechula⁶³, J. Wikne¹⁹, G. Wilk⁷⁸, J. Wilkinson⁹⁷, G.A. Willems¹³⁴, B. Windelband⁹⁴, M. Winn¹²⁶, J.R. Wright¹⁰⁶, W. Wu³⁹, Y. Wu¹¹⁶, R. Xu⁶, A.K. Yadav¹³¹, S. Yalcin⁷¹, Y. Yamaguchi⁹², K. Yamakawa⁹², S. Yang²⁰, S. Yano⁹², Z. Yin⁶, I.-K. Yoo¹⁶, J.H. Yoon⁵⁷, S. Yuan²⁰, A. Yuncu⁹⁴, V. Zaccolo²³, C. Zampolli³², H.J.C. Zanoli⁵⁸, F. Zanone⁹⁴, N. Zardoshti^{32,99}, A. Zarochentsev¹³⁹, P. Závada⁶¹, N. Zaviyalov¹³⁹, M. Zhalov¹³⁹, B. Zhang⁶, S. Zhang³⁹, X. Zhang⁶, Y. Zhang¹¹⁶, M. Zhao¹⁰, V. Zherebchevskii¹³⁹, Y. Zhi¹⁰, N. Zhigareva¹³⁹,

D. Zhou ⁶, Y. Zhou ⁸², J. Zhu ^{97,6}, Y. Zhu⁶, G. Zinovjev^{1,3}, N. Zurlo ^{130,54}

Affiliation Notes

^I Deceased

^{II} Also at: Max-Planck-Institut für Physik, Munich, Germany

^{III} Also at: Italian National Agency for New Technologies, Energy and Sustainable Economic Development (ENEA), Bologna, Italy

^{IV} Also at: Dipartimento DET del Politecnico di Torino, Turin, Italy

^V Also at: Department of Applied Physics, Aligarh Muslim University, Aligarh, India

^{VI} Also at: Institute of Theoretical Physics, University of Wrocław, Poland

^{VII} Also at: An institution covered by a cooperation agreement with CERN

Collaboration Institutes

¹ A.I. Alikhanyan National Science Laboratory (Yerevan Physics Institute) Foundation, Yerevan, Armenia

² AGH University of Krakow, Cracow, Poland

³ Bogolyubov Institute for Theoretical Physics, National Academy of Sciences of Ukraine, Kiev, Ukraine

⁴ Bose Institute, Department of Physics and Centre for Astroparticle Physics and Space Science (CAPSS), Kolkata, India

⁵ California Polytechnic State University, San Luis Obispo, California, United States

⁶ Central China Normal University, Wuhan, China

⁷ Centro de Aplicaciones Tecnológicas y Desarrollo Nuclear (CEADEN), Havana, Cuba

⁸ Centro de Investigación y de Estudios Avanzados (CINVESTAV), Mexico City and Mérida, Mexico

⁹ Chicago State University, Chicago, Illinois, United States

¹⁰ China Institute of Atomic Energy, Beijing, China

¹¹ Chungbuk National University, Cheongju, Republic of Korea

¹² Comenius University Bratislava, Faculty of Mathematics, Physics and Informatics, Bratislava, Slovak Republic

¹³ COMSATS University Islamabad, Islamabad, Pakistan

¹⁴ Creighton University, Omaha, Nebraska, United States

¹⁵ Department of Physics, Aligarh Muslim University, Aligarh, India

¹⁶ Department of Physics, Pusan National University, Pusan, Republic of Korea

¹⁷ Department of Physics, Sejong University, Seoul, Republic of Korea

¹⁸ Department of Physics, University of California, Berkeley, California, United States

¹⁹ Department of Physics, University of Oslo, Oslo, Norway

²⁰ Department of Physics and Technology, University of Bergen, Bergen, Norway

²¹ Dipartimento di Fisica, Università di Pavia, Pavia, Italy

²² Dipartimento di Fisica dell'Università and Sezione INFN, Cagliari, Italy

²³ Dipartimento di Fisica dell'Università and Sezione INFN, Trieste, Italy

²⁴ Dipartimento di Fisica dell'Università and Sezione INFN, Turin, Italy

²⁵ Dipartimento di Fisica e Astronomia dell'Università and Sezione INFN, Bologna, Italy

²⁶ Dipartimento di Fisica e Astronomia dell'Università and Sezione INFN, Catania, Italy

²⁷ Dipartimento di Fisica e Astronomia dell'Università and Sezione INFN, Padova, Italy

²⁸ Dipartimento di Fisica 'E.R. Caianiello' dell'Università and Gruppo Collegato INFN, Salerno, Italy

²⁹ Dipartimento DISAT del Politecnico and Sezione INFN, Turin, Italy

³⁰ Dipartimento di Scienze MIFT, Università di Messina, Messina, Italy

³¹ Dipartimento Interateneo di Fisica 'M. Merlin' and Sezione INFN, Bari, Italy

³² European Organization for Nuclear Research (CERN), Geneva, Switzerland

³³ Faculty of Electrical Engineering, Mechanical Engineering and Naval Architecture, University of Split, Split, Croatia

³⁴ Faculty of Engineering and Science, Western Norway University of Applied Sciences, Bergen, Norway

³⁵ Faculty of Nuclear Sciences and Physical Engineering, Czech Technical University in Prague, Prague, Czech Republic

³⁶ Faculty of Physics, Sofia University, Sofia, Bulgaria

³⁷ Faculty of Science, P.J. Šafárik University, Košice, Slovak Republic

³⁸ Frankfurt Institute for Advanced Studies, Johann Wolfgang Goethe-Universität Frankfurt, Frankfurt, Germany

- ³⁹ Fudan University, Shanghai, China
⁴⁰ Gangneung-Wonju National University, Gangneung, Republic of Korea
⁴¹ Gauhati University, Department of Physics, Guwahati, India
⁴² Helmholtz-Institut für Strahlen- und Kernphysik, Rheinische Friedrich-Wilhelms-Universität Bonn, Bonn, Germany
⁴³ Helsinki Institute of Physics (HIP), Helsinki, Finland
⁴⁴ High Energy Physics Group, Universidad Autónoma de Puebla, Puebla, Mexico
⁴⁵ Horia Hulubei National Institute of Physics and Nuclear Engineering, Bucharest, Romania
⁴⁶ Indian Institute of Technology Bombay (IIT), Mumbai, India
⁴⁷ Indian Institute of Technology Indore, Indore, India
⁴⁸ INFN, Laboratori Nazionali di Frascati, Frascati, Italy
⁴⁹ INFN, Sezione di Bari, Bari, Italy
⁵⁰ INFN, Sezione di Bologna, Bologna, Italy
⁵¹ INFN, Sezione di Cagliari, Cagliari, Italy
⁵² INFN, Sezione di Catania, Catania, Italy
⁵³ INFN, Sezione di Padova, Padova, Italy
⁵⁴ INFN, Sezione di Pavia, Pavia, Italy
⁵⁵ INFN, Sezione di Torino, Turin, Italy
⁵⁶ INFN, Sezione di Trieste, Trieste, Italy
⁵⁷ Inha University, Incheon, Republic of Korea
⁵⁸ Institute for Gravitational and Subatomic Physics (GRASP), Utrecht University/Nikhef, Utrecht, Netherlands
⁵⁹ Institute of Experimental Physics, Slovak Academy of Sciences, Košice, Slovak Republic
⁶⁰ Institute of Physics, Homi Bhabha National Institute, Bhubaneswar, India
⁶¹ Institute of Physics of the Czech Academy of Sciences, Prague, Czech Republic
⁶² Institute of Space Science (ISS), Bucharest, Romania
⁶³ Institut für Kernphysik, Johann Wolfgang Goethe-Universität Frankfurt, Frankfurt, Germany
⁶⁴ Instituto de Ciencias Nucleares, Universidad Nacional Autónoma de México, Mexico City, Mexico
⁶⁵ Instituto de Física, Universidade Federal do Rio Grande do Sul (UFRGS), Porto Alegre, Brazil
⁶⁶ Instituto de Física, Universidad Nacional Autónoma de México, Mexico City, Mexico
⁶⁷ iThemba LABS, National Research Foundation, Somerset West, South Africa
⁶⁸ Jeonbuk National University, Jeonju, Republic of Korea
⁶⁹ Johann-Wolfgang-Goethe Universität Frankfurt Institut für Informatik, Fachbereich Informatik und Mathematik, Frankfurt, Germany
⁷⁰ Korea Institute of Science and Technology Information, Daejeon, Republic of Korea
⁷¹ KTO Karatay University, Konya, Turkey
⁷² Laboratoire de Physique Subatomique et de Cosmologie, Université Grenoble-Alpes, CNRS-IN2P3, Grenoble, France
⁷³ Lawrence Berkeley National Laboratory, Berkeley, California, United States
⁷⁴ Lund University Department of Physics, Division of Particle Physics, Lund, Sweden
⁷⁵ Nagasaki Institute of Applied Science, Nagasaki, Japan
⁷⁶ Nara Women's University (NWU), Nara, Japan
⁷⁷ National and Kapodistrian University of Athens, School of Science, Department of Physics, Athens, Greece
⁷⁸ National Centre for Nuclear Research, Warsaw, Poland
⁷⁹ National Institute of Science Education and Research, Homi Bhabha National Institute, Jatni, India
⁸⁰ National Nuclear Research Center, Baku, Azerbaijan
⁸¹ National Research and Innovation Agency - BRIN, Jakarta, Indonesia
⁸² Niels Bohr Institute, University of Copenhagen, Copenhagen, Denmark
⁸³ Nikhef, National institute for subatomic physics, Amsterdam, Netherlands
⁸⁴ Nuclear Physics Group, STFC Daresbury Laboratory, Daresbury, United Kingdom
⁸⁵ Nuclear Physics Institute of the Czech Academy of Sciences, Husinec-Řež, Czech Republic
⁸⁶ Oak Ridge National Laboratory, Oak Ridge, Tennessee, United States
⁸⁷ Ohio State University, Columbus, Ohio, United States
⁸⁸ Physics department, Faculty of science, University of Zagreb, Zagreb, Croatia
⁸⁹ Physics Department, Panjab University, Chandigarh, India
⁹⁰ Physics Department, University of Jammu, Jammu, India
⁹¹ Physics Department, University of Rajasthan, Jaipur, India

- ⁹² Physics Program and International Institute for Sustainability with Knotted Chiral Meta Matter (SKCM2), Hiroshima University, Hiroshima, Japan
- ⁹³ Physikalisches Institut, Eberhard-Karls-Universität Tübingen, Tübingen, Germany
- ⁹⁴ Physikalisches Institut, Ruprecht-Karls-Universität Heidelberg, Heidelberg, Germany
- ⁹⁵ Physik Department, Technische Universität München, Munich, Germany
- ⁹⁶ Politecnico di Bari and Sezione INFN, Bari, Italy
- ⁹⁷ Research Division and ExtreMe Matter Institute EMMI, GSI Helmholtzzentrum für Schwerionenforschung GmbH, Darmstadt, Germany
- ⁹⁸ Saha Institute of Nuclear Physics, Homi Bhabha National Institute, Kolkata, India
- ⁹⁹ School of Physics and Astronomy, University of Birmingham, Birmingham, United Kingdom
- ¹⁰⁰ Sección Física, Departamento de Ciencias, Pontificia Universidad Católica del Perú, Lima, Peru
- ¹⁰¹ Stefan Meyer Institut für Subatomare Physik (SMI), Vienna, Austria
- ¹⁰² SUBATECH, IMT Atlantique, Nantes Université, CNRS-IN2P3, Nantes, France
- ¹⁰³ Suranaree University of Technology, Nakhon Ratchasima, Thailand
- ¹⁰⁴ Technical University of Košice, Košice, Slovak Republic
- ¹⁰⁵ The Henryk Niewodniczanski Institute of Nuclear Physics, Polish Academy of Sciences, Cracow, Poland
- ¹⁰⁶ The University of Texas at Austin, Austin, Texas, United States
- ¹⁰⁷ Universidad Autónoma de Sinaloa, Culiacán, Mexico
- ¹⁰⁸ Universidade de São Paulo (USP), São Paulo, Brazil
- ¹⁰⁹ Universidade Estadual de Campinas (UNICAMP), Campinas, Brazil
- ¹¹⁰ Universidade Federal do ABC, Santo Andre, Brazil
- ¹¹¹ University of Cape Town, Cape Town, South Africa
- ¹¹² University of Houston, Houston, Texas, United States
- ¹¹³ University of Jyväskylä, Jyväskylä, Finland
- ¹¹⁴ University of Kansas, Lawrence, Kansas, United States
- ¹¹⁵ University of Liverpool, Liverpool, United Kingdom
- ¹¹⁶ University of Science and Technology of China, Hefei, China
- ¹¹⁷ University of South-Eastern Norway, Kongsberg, Norway
- ¹¹⁸ University of Tennessee, Knoxville, Tennessee, United States
- ¹¹⁹ University of the Witwatersrand, Johannesburg, South Africa
- ¹²⁰ University of Tokyo, Tokyo, Japan
- ¹²¹ University of Tsukuba, Tsukuba, Japan
- ¹²² University Politehnica of Bucharest, Bucharest, Romania
- ¹²³ Université Clermont Auvergne, CNRS/IN2P3, LPC, Clermont-Ferrand, France
- ¹²⁴ Université de Lyon, CNRS/IN2P3, Institut de Physique des 2 Infinis de Lyon, Lyon, France
- ¹²⁵ Université de Strasbourg, CNRS, IPHC UMR 7178, F-67000 Strasbourg, France, Strasbourg, France
- ¹²⁶ Université Paris-Saclay, Centre d'Etudes de Saclay (CEA), IRFU, Département de Physique Nucléaire (DPhN), Saclay, France
- ¹²⁷ Université Paris-Saclay, CNRS/IN2P3, IJCLab, Orsay, France
- ¹²⁸ Università degli Studi di Foggia, Foggia, Italy
- ¹²⁹ Università del Piemonte Orientale, Vercelli, Italy
- ¹³⁰ Università di Brescia, Brescia, Italy
- ¹³¹ Variable Energy Cyclotron Centre, Homi Bhabha National Institute, Kolkata, India
- ¹³² Warsaw University of Technology, Warsaw, Poland
- ¹³³ Wayne State University, Detroit, Michigan, United States
- ¹³⁴ Westfälische Wilhelms-Universität Münster, Institut für Kernphysik, Münster, Germany
- ¹³⁵ Wigner Research Centre for Physics, Budapest, Hungary
- ¹³⁶ Yale University, New Haven, Connecticut, United States
- ¹³⁷ Yonsei University, Seoul, Republic of Korea
- ¹³⁸ Zentrum für Technologie und Transfer (ZTT), Worms, Germany
- ¹³⁹ Affiliated with an institute covered by a cooperation agreement with CERN
- ¹⁴⁰ Affiliated with an international laboratory covered by a cooperation agreement with CERN.